Journal of Applied Mathematics and Computing (2025) 71:3399–3427
https://doi.org/10.1007/s12190-024-02340-9

ORIGINAL RESEARCH

Efficient uniformly convergent numerical methods for singularly perturbed parabolic reaction–diffusion systems with discontinuous source term

Aishwarya Jaiswal[1] · Sunil Kumar[1] · Higinio Ramos[2,3]

Received: 8 August 2024 / Revised: 7 December 2024 / Accepted: 19 December 2024 /
Published online: 11 January 2025

Abstract
This article is concerned with the construction and analysis of efficient uniformly convergent methods for a class of parabolic systems of coupled singularly perturbed reaction–diffusion problems with discontinuous source term. Due to the discontinuity in the source term, the solution to this problem exhibits interior layers along with boundary layers, which are overlapping and interacting in nature. To achieve an efficient numerical solution for the coupled system under consideration, at interior points (excluding the interface point) we employ a special finite difference scheme in time (where the components of the approximate solution are decoupled at each time level) and the central difference scheme in space; for mesh points on the interface, a special finite difference scheme decoupling the components of the approximate solution is developed. A rigorous error analysis is provided, establishing the method's uniform convergence. In terms of computational cost, our numerical methods are more efficient than existing approaches for solving this class of problems. Finally, we provide numerical results to substantiate the theory and showcase the efficiency of our methods.

Keywords Reaction–diffusion problems · Discontinuous data · Interface problems · Multiscale problems · Boundary and interior layers · Computational efficiency · Uniformly convergent

✉ Higinio Ramos
higra@usal.es

Aishwarya Jaiswal
aishwaryajaiswal.rs.mat21@itbhu.ac.in

Sunil Kumar
skumar.mat@iitbhu.ac.in

1 Department of Mathematical Sciences, Indian Institute of Technology (BHU), Varanasi, Uttar Pradesh, India

2 Scientific Computing Group, Universidad de Salamanca, Plaza de la Merced, 37008 Salamanca, Spain

3 Escuela Politécnica Superior de Zamora, Campus Viriato, 49022 Zamora, Spain

1 Introduction

In this work, we consider a 1D coupled system of p (≥ 2) parabolic reaction diffusion equations with discontinuity in the source term, on the domain $G = (0, 1) \times (0, T]$. Specifically, we assume that the source term possesses a single discontinuity at $x = d,\ 0 < d < 1$. Suppose $G_1 = (0, d) \times (0, T]$ and $G_2 = (d, 1) \times (0, T]$. The goal is to find $u \in C^0(\overline{G}) \cap C^{1+l}(G) \cap C^{4+l}(G_1 \cup G_2),\ 0 < l \leq 1$, such that

$$\boldsymbol{L u} := \frac{\partial \boldsymbol{u}}{\partial t} - \boldsymbol{\mathcal{D}_\varepsilon} \frac{\partial^2 \boldsymbol{u}}{\partial x^2} + \boldsymbol{A u} = \boldsymbol{f}, \quad (x, t) \in G_1 \cup G_2, \tag{1}$$

$$\boldsymbol{u}(x, 0) = \mathbf{0}, \quad \boldsymbol{u}(0, t) = \mathbf{0}, \quad \boldsymbol{u}(1, t) = \mathbf{0}, \quad \text{for all} \quad t \in (0, T], \tag{2}$$

where $\boldsymbol{A}(x, t) = \left(a_{ij}(x, t)\right)_{p\times p}$ is a matrix-valued coefficient, $\boldsymbol{f}(x, t) = (f_i(x, t))_{p\times 1}$, is a vector-valued right hand side, and $\boldsymbol{\mathcal{D}_\varepsilon} = \operatorname{diag}\left(\varepsilon_1, \ldots, \varepsilon_p\right)$ is a diagonal matrix with $0 < \varepsilon_1 < \cdots < \varepsilon_p \ll 1$. Furthermore, $\boldsymbol{f}$ exhibits a discontinuity at $x = d$, and the reaction coefficient matrix $\boldsymbol{A}$ is sufficiently smooth, satisfying

$$\begin{aligned} &a_{ii}(x, t) > \sum_{j\neq i, j=1}^{p} \left|a_{ij}(x, t)\right|, \quad \text{for} \quad 1 \leq i \leq p, \\ &a_{ij}(x, t) \leq 0 \quad \text{for} \quad i \neq j, \quad 1 \leq i, j \leq p \end{aligned} \tag{3}$$

and

$$\min_{\substack{(x,t)\in\overline{G}\\ 1\leq i\leq p}} \sum_{j=1}^{p} a_{ij}(x, t) > \alpha > 0, \tag{4}$$

for some constant α. Additionally, the following interface conditions $[u_i](d, t) = 0,\ \varepsilon_i[\frac{\partial u_i}{\partial x}](d, t) = 0$ are satisfied by the exact solution $\boldsymbol{u} = \left(u_1, u_2, \ldots, u_p\right)^T$, where the jump at some point (d, t) in any function is expressed as $[\omega](d, t) = \omega(d+, t) - \omega(d-, t)$.

Singularly perturbed equations typically involve a small positive parameter that multiplies some or all of the coefficients of the higher-order derivative terms [6, 16–18, 24, 26]. One of the reasons for taking SPPs into consideration is their wide application in fluid dynamics, chemical kinetics, physics, mathematical biology, or engineering. The term “singular perturbation" refers to the rapid changes in the solution behavior as the perturbation parameter approaches zero, giving rise to mathematical manifestations of layers, specifically boundary or interior layers. Boundary layers are notable for their interactive and overlapping nature, especially in coupled systems, where different small parameters are present in each equation. On the other hand, interior layers arise primarily due to non-smoothness in the data, presenting intriguing challenges. This article primarily focuses on approximating a system of coupled singularly perturbed equations of reaction–diffusion type with a discontinuous source term that exhibits boundary and interior layers.

Throughout the early twentieth century, researchers have diligently explored numerical techniques for singularly perturbed problems (SPPs), contributing to an ever-expanding research frontier [1, 3, 4, 8, 10–15, 19]. Classical numerical approaches often struggle to achieve accurate approximations of the exact solution of SPPs on uniform meshes for small values of the perturbation parameter. This highlights the need to develop numerical methods that can produce reliable and accurate approximate solutions, regardless of the perturbation parameter values. These methods are known as parameter uniform/uniformly convergent numerical methods. For coupled systems with non-smooth data, the scenario can become quite intricate. When parameters of different magnitudes are associated with each equation, the solution develops interactive and overlapping boundary and interior layers. This complexity adds difficulty to both the development of numerical methods and the subsequent numerical analysis.

In recent years, singular perturbation problems with non-smooth data have been successful in drawing the attention of many researchers (see [3, 5, 7, 20, 21, 23, 25, 28] and the references therein). However, the numerical treatment of problem (1)–(2) is still in its infancy stage. The authors in [22] presented a uniformly convergent numerical method for problem (1)–(2) using the implicit Euler scheme in time and central difference approximation in space. However, the computational cost of this method is high due to the need to solve a coupled system at each time level. To the best of our knowledge, we are not aware of any attempts to develop and analyze computationally efficient numerical methods for singularly perturbed coupled systems of parabolic reaction–diffusion problems with discontinuous data, which exhibit interactive and overlapping boundary and interior layers.

In this paper, our aim is to develop and analyze computationally efficient numerical methods for coupled systems of parabolic reaction–diffusion problems (1)–(2) with discontinuous source term. We employ a uniform mesh in time and an appropriate layer adapted Shishkin mesh in space. To achieve an efficient numerical solution for the coupled system under consideration, at interior points (excluding the interface point) we employ a special finite difference scheme in time (where the components of the approximate solution are decoupled at each time level) and the central difference scheme in space; for mesh points on the interface a special finite difference scheme is developed. We then proceed with error analysis to demonstrate that the proposed numerical methods are uniformly convergent. Our discretization requires solving tridiagonal linear systems at each time level. Hence, in terms of computational cost, our numerical methods are more efficient compared to existing methods for the problem at hand. Numerical examples substantiate the theoretical results and showcase the methods' efficiency.

This article is structured as follows. Section 2 presents the estimates of the smooth and layer components and also of their derivatives. Section 3 introduces novel computationally efficient numerical methods for solving the concerned problem. Section 4 handles the error analysis. In Sect. 5, some numerical results are presented, confirming the theoretically proven order of convergence of the proposed methods. Additionally, we present a comparison with standard discretization techniques.

Notations: We define $\boldsymbol{y} = (y_1, y_2, \ldots, y_p)^T$, $|\boldsymbol{y}| = (|y_1|, |y_2|, \ldots, |y_p|)^T$, and $\boldsymbol{y}_{i,n} = \boldsymbol{y}(x_i, t_n) = (y_1(x_i, t_n),\ y_2(x_i, t_n), \ldots, y_p(x_i, t_n))^T$. For $\boldsymbol{y}, \boldsymbol{z} \in C(\overline{G})^p$, $\boldsymbol{y} \le \boldsymbol{z}$ if

$y_k \leq z_k$, $1 \leq k \leq p$; if $y \in C(\overline{G})$ then $y_{i,n} = y(x_i, t_n)$. Henceforth, the scalar C and vector $\boldsymbol{C} = (C, C, \ldots, C)^T$ are assumed to be generic positive constants which are independent of the diffusion parameters ε_i, $1 \leq i \leq p$, and the discretization parameters. $\|.\|_R$ represents the maximum norm on any closed subset R of $[0, 1] \times [0, T]$. Further, the notation $\|.\|_{R^{N,M}}$ is considered for the maximum norm in a discrete domain.

2 Bounds on the derivatives

Here, we provide bounds on the derivatives required for the convergence analysis of the proposed methods.

Lemma 1 *Suppose $\boldsymbol{u}$ is the exact solution of problem (1)–(2). Then, for $i = 1, \ldots, p$, and $(x, t) \in G_1 \cup G_2$, we have*

$$\|\boldsymbol{u}\|_{\overline{G}} \leq \max\left\{\|\boldsymbol{u}\|_{\overline{G}\setminus G}, \frac{1}{\alpha}\|\boldsymbol{L}\boldsymbol{u}\|_{G_1\cup G_2}\right\},$$

$$\left|\frac{\partial^s u_i}{\partial t^s}(x,t)\right| \leq C\left(\|\boldsymbol{u}\|_{\overline{G}\setminus G} + \sum_{q=0}^{s}\left\|\frac{\partial^q \boldsymbol{f}}{\partial t^q}\right\|_{G_1\cup G_2}\right), \quad s = 0, 1, 2,$$

$$\left|\frac{\partial^s u_i}{\partial x^s}(x,t)\right| \leq C\varepsilon_i^{-\frac{s}{2}}\left(\|\boldsymbol{u}\|_{\overline{G}\setminus G} + \|\boldsymbol{f}\|_{G_1\cup G_2} + \left\|\frac{\partial \boldsymbol{f}}{\partial t}\right\|_{G_1\cup G_2}\right), \quad s = 1, 2,$$

$$\left|\frac{\partial^s u_i}{\partial x^s}(x,t)\right| \leq C\varepsilon_i^{-1}\varepsilon_i^{\frac{-(s-2)}{2}}\left(\|\boldsymbol{u}\|_{\overline{G}\setminus G} + \|\boldsymbol{f}\|_{G_1\cup G_2} + \left\|\frac{\partial \boldsymbol{f}}{\partial t}\right\|_{G_1\cup G_2} + \left\|\frac{\partial^2 \boldsymbol{f}}{\partial t^2}\right\|_{G_1\cup G_2}\right.$$
$$\left. + \varepsilon_i^{(s-2)/2}\left\|\frac{\partial^{s-2} \boldsymbol{f}}{\partial t^{s-2}}\right\|_{G_1\cup G_2}\right),$$

$s = 3, 4,$ *and*

$$\left|\frac{\partial^s u_i}{\partial x^{s-1}\partial t}(x,t)\right| \leq C\varepsilon_i^{\frac{(1-s)}{2}}\left(\|\boldsymbol{u}\|_{\overline{G}\setminus G} + \|\boldsymbol{f}\|_{G_1\cup G_2} + \left\|\frac{\partial \boldsymbol{f}}{\partial t}\right\|_{G_1\cup G_2} + \left\|\frac{\partial^2 \boldsymbol{f}}{\partial t^2}\right\|_{G_1\cup G_2}\right),$$

$s = 2, 3.$

Proof The lemma can be proved using the arguments presented in [22]. □

The reduced form of the problem given in (1)–(2) is

$$\frac{\partial \boldsymbol{u}_0}{\partial t} + \boldsymbol{A}\boldsymbol{u}_0 = \boldsymbol{f}, \quad (x,t) \in G_1 \cup G_2,$$
$$\boldsymbol{u}_0(x, 0) = \boldsymbol{0}.$$

For obtaining precise bounds on the derivatives, the analytical solution is split into components, comprising of a smooth component $\boldsymbol{y}$ and a layer component $\boldsymbol{z}$, i.e.,

$\boldsymbol{u} = \boldsymbol{y} + \boldsymbol{z}$. The smooth component $\boldsymbol{y}$ satisfies the parabolic problem

$$
\begin{aligned}
&\boldsymbol{L}\boldsymbol{y}(x,t) = \boldsymbol{f}(x,t), \quad (x,t) \in G_1 \cup G_2,\\
&\boldsymbol{y}(0,t) = \boldsymbol{u}_0(0,t), \quad \boldsymbol{y}(d-,t) = \boldsymbol{u}_0(d-,t),\\
&\boldsymbol{y}(d+,t) = \boldsymbol{u}_0(d+,t), \quad \boldsymbol{y}(1,t) = \boldsymbol{u}_0(1,t), \quad \boldsymbol{y}(x,0) = \boldsymbol{0}.
\end{aligned}
$$

The layer component $\boldsymbol{z}$ satisfies the parabolic problem

$$
\begin{aligned}
&\boldsymbol{L}\boldsymbol{z}(x,t) = \boldsymbol{0}, \quad (x,t) \in G_1 \cup G_2,\\
&\boldsymbol{z}(0,t) = (\boldsymbol{u} - \boldsymbol{y})(0,t), \quad \boldsymbol{z}(1,t) = (\boldsymbol{u} - \boldsymbol{y})(1,t),\\
&[\boldsymbol{z}](d,t) = -[\boldsymbol{y}](d,t), \quad \boldsymbol{z}(x,0) = \boldsymbol{0}, \quad [\boldsymbol{z}_x](d,t) = -\left[\boldsymbol{y}_x\right](d,t).
\end{aligned}
$$

Here, $\boldsymbol{z}$ satisfies the interface conditions since $\boldsymbol{u}$ satisfies the interface conditions

$$[\boldsymbol{u}](d,t) = \boldsymbol{0}, \quad [\boldsymbol{u}_x](d,t) = \boldsymbol{0}.$$

For bounding the derivatives, the following boundary layer functions are defined for $1 \le i \le p$:

$$
\begin{aligned}
B^l_{\varepsilon_i}(x) &= e^{\left(-x\sqrt{\alpha/\varepsilon_i}\right)} + e^{\left(-(d-x)\sqrt{\alpha/\varepsilon_i}\right)},\\
B^r_{\varepsilon_i}(x) &= e^{\left((d-x)\sqrt{\alpha/\varepsilon_i}\right)} + e^{\left(-(1-x)\sqrt{\alpha/\varepsilon_i}\right)}.
\end{aligned}
\tag{5}
$$

Lemma 2 *Suppose that the coupling matrix $\boldsymbol{A}(x,t)$ satisfies conditions (3)–(4). Then, for $(x,t) \in G_1 \cup G_2$, $i = 1,\ldots,p$, the following bounds hold for the regular component $\mathbf{y}$ and the layer component $\mathbf{z}$ of the analytical solution $\mathbf{u}$ and their corresponding derivatives:*

$$
\begin{aligned}
&\left|\frac{\partial^s y_i}{\partial t^s}(x,t)\right|_{G_1\cup G_2} \le C, \quad \text{for } s = 0,1,2,\\
&\left|\frac{\partial^s y_i}{\partial x^s}(x,t)\right|_{G_1\cup G_2} \le \begin{cases} C(1+\varepsilon_i^{(1-\frac{s}{2})}B^l_{\varepsilon_i}(x)), & (x,t)\in G_1,\\ C(1+\varepsilon_i^{(1-\frac{s}{2})}B^r_{\varepsilon_i}(x)), & (x,t)\in G_2, \end{cases} \quad \text{for } s = 0,1,2,3,4, \quad \text{and}\\
&\left|\frac{\partial^s y_i}{\partial x^{s-1}\partial t}(x,t)\right|_{G_1\cup G_2} \le C \quad \text{for } s = 2,3;
\end{aligned}
$$

and

$$\left|\frac{\partial^s z_i}{\partial t^s}(x,t)\right| \le \begin{cases} CB^l_{\varepsilon_p}(x), & (x,t)\in G_1, \\ CB^r_{\varepsilon_p}(x), & (x,t)\in G_2, \end{cases} \quad \textit{for} \quad s=0,1,2,$$

$$\left|\frac{\partial^s z_i}{\partial x^s}(x,t)\right| \le \begin{cases} C\sum_{q=1}^p \frac{B^l_{\varepsilon_q}(x)}{\varepsilon_q^{\frac{s}{2}}}, & (x,t)\in G_1, \\ C\sum_{q=1}^p \frac{B^r_{\varepsilon_q}(x)}{\varepsilon_q^{\frac{s}{2}}}, & (x,t)\in G_2, \end{cases} \quad \textit{for} \quad s=1,2,$$

$$\left|\frac{\partial^3 z_i}{\partial x^3}(x,t)\right| \le \begin{cases} C\sum_{q=1}^p \frac{B^l_{\varepsilon_q}(x)}{\varepsilon_q^{\frac{3}{2}}}, & (x,t)\in G_1, \\ C\sum_{q=1}^p \frac{B^r_{\varepsilon_q}(x)}{\varepsilon_q^{\frac{3}{2}}}, & (x,t)\in G_2, \end{cases}$$

$$\left|\varepsilon_i\frac{\partial^4 z_i}{\partial x^4}(x,t)\right| \le \begin{cases} C\sum_{q=1}^p \frac{B^l_{\varepsilon_q}(x)}{\varepsilon_q}, & (x,t)\in G_1, \\ C\sum_{q=1}^p \frac{B^r_{\varepsilon_q}(x)}{\varepsilon_q}, & (x,t)\in G_2, \end{cases}$$

$$\left|\frac{\partial^s z_i}{\partial x^{s-1}\partial t}(x,t)\right| \le \varepsilon_i^{\frac{(1-s)}{2}} C\left(\|\boldsymbol{u}\|_{\overline{G}\setminus G} + \|\boldsymbol{f}\|_{G_1\cup G_2} + \left\|\frac{\partial \boldsymbol{f}}{\partial t}\right\|_{G_1\cup G_2} + \left\|\frac{\partial^2 \boldsymbol{f}}{\partial t^2}\right\|_{G_1\cup G_2}\right),$$
$$s=2,3.$$

Proof The proof of the lemma can be done using the arguments in [22]. □

For analyzing the robust convergence of the proposed schemes, we need precise bounds on the regular and singular components, which are given in the following lemma.

Lemma 3 *Suppose that the reaction matrix $\boldsymbol{A}(x,t)$ satisfies conditions (3)–(4). Then, for $(x,t)\in G_1\cup G_2$, $i=1,\dots,p$, and $\hat{s}=0,1,2,3$, the following estimates hold for the smooth component $\mathbf{y}$ and its derivatives:*

$$\left|\frac{\partial^{\hat{s}} y_i}{\partial x^{\hat{s}}}(x,t)\right|_{G_1\cup G_2} \le \begin{cases} C\left(1+\sum_{q=i}^p \frac{B^l_{\varepsilon_q}(x)}{\varepsilon_q^{\frac{\hat{s}}{2}-1}}\right), & (x,t)\in G_1, \\ C\left(1+\sum_{q=i}^p \frac{B^r_{\varepsilon_q}(x)}{\varepsilon_q^{\frac{\hat{s}}{2}-1}}\right), & (x,t)\in G_2. \end{cases}$$

Furthermore, the singular component can be decomposed as $z_i(x,t) = \sum_{q=1}^{s+1} z_{i,\varepsilon_q}(x,t) = \sum_{q=1}^{s+1} w_{i,\varepsilon_q}(x,t)$, where

$$\left|\frac{\partial^2 z_{i,\varepsilon_q}}{\partial x^2}(x,t)\right| \le C\begin{cases} \frac{B^l_{\varepsilon_q}(x)}{\varepsilon_q}, & (x,t)\in G_1, \\ \frac{B^r_{\varepsilon_q}(x)}{\varepsilon_q}, & (x,t)\in G_2, \end{cases}$$

$$\left|\frac{\partial^3 z_{i,\varepsilon_q}}{\partial x^3}(x,t)\right| \le C\begin{cases} \frac{B^l_{\varepsilon_q}(x)}{\varepsilon_q^{3/2}}, & (x,t)\in G_1, \\ \frac{B^r_{\varepsilon_q}(x)}{\varepsilon_q^{3/2}}, & (x,t)\in G_2, \end{cases}$$

$$\left|\varepsilon_i \frac{\partial^2 w_{i,\varepsilon_q}}{\partial x^2}(x,t)\right| \le C \begin{cases} B^l_{\varepsilon_q}(x), & (x,t)\in G_1, \\ B^r_{\varepsilon_q}(x), & (x,t)\in G_2, \end{cases}$$

$$\left|\varepsilon_i \frac{\partial^3 w_{i,\varepsilon_q}}{\partial x^3}(x,t)\right| \le C \begin{cases} \frac{B^l_{\varepsilon_q}(x)}{\sqrt{\varepsilon_q}}, & (x,t)\in G_1, \\ \frac{B^r_{\varepsilon_q}(x)}{\sqrt{\varepsilon_q}}, & (x,t)\in G_2, \end{cases}$$

$$\left|\varepsilon_i \frac{\partial^4 w_{i,\varepsilon_q}}{\partial x^4}(x,t)\right| \le C \begin{cases} \frac{B^l_{\varepsilon_q}(x)}{\varepsilon_q}, & (x,t)\in G_1, \\ \frac{B^r_{\varepsilon_q}(x)}{\varepsilon_q}, & (x,t)\in G_2. \end{cases}$$

Proof See [22] for the bounds of the regular component. The arguments outlined in Lemma 13 of [8] can be used to complete the proof for the bounds of the singular component. □

3 Discretization of the problem

This section introduces the discretization of problem (1)–(2). We consider a non-uniform (piecewise uniform) Shishkin mesh Ω^N in space:

$$\Omega^N = \left\{x_i : 1 \le i \le \frac{N}{2} - 1\right\} \cup \left\{x_i : \frac{N}{2} + 1 \le i \le N-1\right\},$$

and a uniform mesh $\mathcal{T}^M = \{\ t_n = n\tau \colon 1 \le n \le M,\ \tau = T/M\ \}$ in time. Thus, $\overline{\Omega}^N = \Omega^N \cup \{x_0 = 0,\ x_N = 1\}$ represents the spatial mesh and $\overline{\mathcal{T}}^M = \mathcal{T}^M \cup \{t_0 = 0\}$ is the temporal mesh. Further, we denote the mesh by $\overline{G}^{N,M} = \overline{\Omega}^N \times \overline{\mathcal{T}}^M$ and $G^{N,M} = \overline{G}^{N,M} \cap G$. The non-uniform Shishkin mesh is constructed with the help of transition parameters, defined as follows

$$\sigma^l_{\varepsilon_p} := \min\left\{\frac{d}{4}, 2\sqrt{\frac{\varepsilon_p}{\alpha}}\ln N\right\}, \quad \sigma^r_{\varepsilon_p} := \min\left\{\frac{(1-d)}{4}, 2\sqrt{\frac{\varepsilon_p}{\alpha}}\ln N\right\},$$
$$\sigma^l_{\varepsilon_s} := \min\left\{\frac{\sigma^l_{\varepsilon_{s+1}}}{4}, 2\sqrt{\frac{\varepsilon_s}{\alpha}}\ln N\right\}, \quad \sigma^r_{\varepsilon_s} := \min\left\{\frac{\sigma^r_{\varepsilon_{s+1}}}{4}, 2\sqrt{\frac{\varepsilon_s}{\alpha}}\ln N\right\},$$

for $s = p-1, \ldots, 2, 1$. Let $h_i = x_i - x_{i-1}$ denote the mesh spacing in the spatial direction. Let $\bar{h}_i = \frac{(h_i + h_{i+1})}{2}$, $x_{\frac{N}{2}} = d$, and $\overline{\Omega}^N := \{x_i \colon i = 0, 1, 2, \ldots, N\}$. Suppose $N = 2^l$, where $l \ge 5$ is a positive integer.

The subdomain $[0, d]$ is partitioned into $2p+1$ subintervals to get

$$\left[0, \sigma^l_{\varepsilon_1}\right] \cup \cdots \cup \left[\sigma^l_{\varepsilon_{p-1}}, \sigma^l_{\varepsilon_p}\right] \cup \left[\sigma^l_{\varepsilon_p}, d - \sigma^l_{\varepsilon_p}\right] \cup \left[d - \sigma^l_{\varepsilon_p}, d - \sigma^l_{\varepsilon_{p-1}}\right]$$
$$\cup \cdots \cup \left[d - \sigma^l_{\varepsilon_1}, d\right].$$

The subintervals $[0, \sigma^l_{\varepsilon_1}]$ and $[d - \sigma^l_{\varepsilon_1}, d]$ are divided according to an equidistant mesh consisting of $(N/2^{p+2} + 1)$ mesh points. On the sub-intervals $[\sigma^l_{\varepsilon_s}, \sigma^l_{\varepsilon_{s+1}}]$ and $[d - \sigma^l_{\varepsilon_{s+1}}, d - \sigma^l_{\varepsilon_s}]$, for $1 \leq s \leq p-1$, an equidistant mesh with $(N/2^{p-s+3} + 1)$ mesh points is considered, and on $[\sigma^l_{\varepsilon_p}, d - \sigma^l_{\varepsilon_p}]$ an equidistant mesh with $(N/4+1)$ mesh points is used.

Similarly, the subdomain $[d, 1]$ is partitioned into $2p+1$ subintervals as

$$\left[d, d + \sigma^r_{\varepsilon_1}\right] \cdots \cup \left[d + \sigma^r_{\varepsilon_p}, 1 - \sigma^r_{\varepsilon_p}\right] \cup \left[1 - \sigma^r_{\varepsilon_p}, 1 - \sigma^r_{\varepsilon_{p-1}}\right] \cup \left[1 - \sigma^r_{\varepsilon_{p-1}}, 1 - \sigma^r_{\varepsilon_{p-2}}\right] \cup \cdots \cup [1 - \sigma^r_{\varepsilon_1}, 1].$$

The subintervals $[d, d + \sigma^r_{\varepsilon_1}]$ and $[1 - \sigma^r_{\varepsilon_1}, 1]$ are divided according to an equidistant mesh consisting of $(N/2^{p+2}+1)$ mesh points. On the sub-intervals $[d+\sigma^r_{\varepsilon_s}, d+\sigma^r_{\varepsilon_{s+1}}]$ and $[1-\sigma^r_{\varepsilon_{s+1}}, 1-\sigma^r_{\varepsilon_s}]$, for $1 \leq s \leq p-1$, an equidistant mesh with $(N/2^{p-s+3}+1)$ mesh points is used and on $[d + \sigma^r_{\varepsilon_p}, 1 - \sigma^r_{\varepsilon_p}]$ an equidistant mesh with $(N/4+1)$ mesh points is placed.

Next, taking into consideration the following data

$$\boldsymbol{U}(0, t_n) = \boldsymbol{u}(0, t_n), \quad \boldsymbol{U}(1, t_n) = \boldsymbol{u}(1, t_n), \quad \boldsymbol{U}(x_i, 0) = \boldsymbol{u}(x_i, 0), \tag{6}$$

we define the finite difference scheme along the non-interface line given by

$$\boldsymbol{L}^{N,M}\boldsymbol{U}^n_i = \boldsymbol{f}^n_i, \quad \forall (x_i, t_n) \in G^{N,M} \setminus \left\{(d, t_n) : t_n \in \mathcal{T}^M\right\}, \tag{7}$$

and for the points $(x_{\frac{N}{2}}, t_n) = (d, t_n)$, for $t_n \in \mathcal{T}^M$, we consider the following discretization

$$\boldsymbol{L}^{N,M}\boldsymbol{U}^n_d = \overline{\boldsymbol{f}}^n_d, \tag{8}$$

where

$$\overline{\boldsymbol{f}}^n_d = \overline{\boldsymbol{f}}(d, t_n) = \frac{h_{\frac{N}{2}} f(d - h_{\frac{N}{2}}, t_n) + h_{\frac{N}{2}+1} f(d + h_{\frac{N}{2}}, t_n)}{h_{\frac{N}{2}} + h_{\frac{N}{2}+1}}.$$

Here, with the help of the difference operators

$$\delta^2_x \boldsymbol{W}^n_r = \frac{2}{h_r + h_{r+1}}\left(\frac{\boldsymbol{W}^n_{r+1} - \boldsymbol{W}^n_r}{h_{r+1}} - \frac{\boldsymbol{W}^n_r - \boldsymbol{W}^n_{r-1}}{h_r}\right), \quad D^-_t \boldsymbol{W}^n_r = \frac{\boldsymbol{W}^n_r - \boldsymbol{W}^{n-1}_r}{\tau},$$
$$D^-_x \boldsymbol{W}^n_r = \frac{\boldsymbol{W}^n_r - \boldsymbol{W}^n_{r-1}}{h_r},$$

the discrete operator $\boldsymbol{L}^{N,M}$ is defined as

$$\boldsymbol{L}^{N,M}\boldsymbol{U}^n_i := \boldsymbol{D}^-_t \boldsymbol{U}^n_i - \boldsymbol{\mathcal{D}}_{\boldsymbol{\varepsilon}} \delta^2_x \boldsymbol{U}^n_i + \boldsymbol{\mathcal{M}}^n_i \boldsymbol{U}^n_i - \boldsymbol{\mathcal{N}}^n_i \boldsymbol{U}^{n-1}_i, \tag{9}$$

where $\boldsymbol{A}_i^n = \boldsymbol{\mathcal{M}}_i^n - \boldsymbol{\mathcal{N}}_i^n$ with $\boldsymbol{A}_i^n = \boldsymbol{A}(x_i, t_n)$. We note that in [22], the classical implicit Euler scheme is used, which corresponds to the choice

$$\boldsymbol{\mathcal{M}}_i^n = \boldsymbol{A}_i^n. \tag{10}$$

Here, we consider two efficient schemes to solve the parabolic problem with a discontinuous source term, which correspond to the following choices of $\boldsymbol{\mathcal{M}}_i^n$ [2, 9, 27, 29]:

$$\boldsymbol{\mathcal{M}}_i^n \in \left\{ \begin{pmatrix} a_{11}(x_i, t_n) & 0 & 0 & \cdots & 0 \\ 0 & a_{22}(x_i, t_n) & 0 & \cdots & 0 \\ 0 & 0 & a_{33}(x_i, t_n) & \cdots & 0 \\ \vdots & \vdots & \vdots & \ddots & \vdots \\ 0 & 0 & 0 & \cdots & a_{pp}(x_i, t_n) \end{pmatrix}, \begin{pmatrix} a_{11}(x_i, t_n) & 0 & 0 & \cdots & 0 \\ a_{21}(x_i, t_n) & a_{22}(x_i, t_n) & 0 & \cdots & 0 \\ a_{31}(x_i, t_n) & a_{32}(x_i, t_n) & a_{33}(x_i, t_n) & \cdots & 0 \\ \vdots & \vdots & \vdots & \ddots & \vdots \\ a_{p1}(x_i . t_n) & a_{p2}(x_i, t_n) & a_{p3}(x_i, t_n) & \cdots & a_{pp}(x_i, t_n) \end{pmatrix} \right\}, \tag{11}$$

that is we consider $\boldsymbol{\mathcal{M}}_i^n$ to be the diagonal matrix $(diag(\boldsymbol{A}_i^n))$, or to be the lower triangular matrix $(trial(\boldsymbol{A}_i^n))$, associated to $\boldsymbol{A}_i^n$. Note that the works [2, 9, 27, 29] are limited to problems with a continuous source term.

The following two lemmas are the implication of the inverse positivity property of the matrix generated using the discrete scheme.

Lemma 4 *Let* $\boldsymbol{V}$ *be a mesh function satisfying* $\boldsymbol{V} \geq \boldsymbol{0}$ *for* $(x_i, t_n) \in \overline{G}^{N,M} \setminus G^{N,M}$ *and* $\boldsymbol{L}^{N,M}\ \boldsymbol{V} \geq \boldsymbol{0}\ \forall\ (x_i, t_n) \in G^{N,M}$. *Then* $\boldsymbol{V} \geq \boldsymbol{0}$ *for all* $(x_i, t_n) \in \overline{G}^{N,M}$.

Lemma 5 *Let* $\boldsymbol{U}$ *denote the solution of* (7)–(6). *Then*

$$\|\boldsymbol{U}\|_{\overline{G}^{N,M}} \leq \max \left\{ \|\boldsymbol{U}\|_{\overline{G}^{N,M} \setminus G^{N,M}}, \frac{1}{\alpha} \|\boldsymbol{f}\|_{G_1^{N,M} \cup G_2^{N,M}} \right\}.$$

4 Analysis of the discretization

The truncation error bounds for the proposed discretization are obtained using the estimates given below, which are obtained using Taylor expansions for a smooth function ψ. For $i = 1, 2, \ldots, \frac{N}{2} - 1, \frac{N}{2} + 1, \ldots, N$ and $n = 1, 2, \ldots, M$, we get

$$\left| \left(\frac{\partial}{\partial t} - D_t^- \right) \psi(x_i, t_n) \right| \leq C (t_n - t_{n-1}) \max_{s \in [t_{n-1}, t_n]} \left| \frac{\partial^2 \psi}{\partial t^2}(x_i, s) \right|, \tag{12}$$

$$\left| \left(\frac{\partial^2}{\partial x^2} - \delta_x^2 \right) \psi(x_i, t_n) \right| \leq C \max_{s \in [x_{i-1}, x_{i+1}]} \left| \frac{\partial^2 \psi}{\partial x^2}(s, t_n) \right|, \tag{13}$$

$$\left|\left(\frac{\partial^2}{\partial x^2}-\delta_x^2\right)\psi\left(x_i,t_n\right)\right| \le C\left(x_{i+1}-x_{i-1}\right)\max_{s\in\left[x_{i-1},x_{i+1}\right]}\left|\frac{\partial^3\psi}{\partial x^3}\left(s,t_n\right)\right|, \quad (14)$$

$$\left|\left(\frac{\partial^2}{\partial x^2}-\delta_x^2\right)\psi\left(x_i,t_n\right)\right| \le C\left(x_{i+1}-x_{i-1}\right)^2\max_{s\in\left[x_{i-1},x_{i+1}\right]}\left|\frac{\partial^4\psi}{\partial x^4}\left(s,t_n\right)\right|. \quad (15)$$

For the smooth component we have

$$\begin{aligned}&\left(\boldsymbol{L}^{N,M}\boldsymbol{y}-\boldsymbol{L}\boldsymbol{y}\right)\left(x_i,t_n\right)\\&=(D_t^-\boldsymbol{y}-\frac{\partial\boldsymbol{y}}{\partial t})(x_i,t_n)+\mathcal{E}\left(\frac{\partial^2\boldsymbol{y}}{\partial x^2}-\delta_x^2\boldsymbol{y}\right)\left(x_i,t_n\right)+\boldsymbol{\mathcal{N}}_i^n(\boldsymbol{y}(x_i,t_n)-\boldsymbol{y}(x_i,t_{n-1})).\end{aligned}$$

Now, using (12) and bounds from Lemma 2, we obtain

$$\left|(D_t^-\boldsymbol{y}-\frac{\partial\boldsymbol{y}}{\partial t})(x_i,t_n)\right| \le C\tau\max_{s\in\left[t_{n-1},t_n\right]}\left|\frac{\partial^2\boldsymbol{y}}{\partial t^2}\left(x_i,s\right)\right| \le \boldsymbol{C}M^{-1},$$

and

$$\left|\boldsymbol{\mathcal{N}}_i^n(\boldsymbol{y}(x_i,t_n)-\boldsymbol{y}(x_i,t_{n-1}))\right| \le C\tau\max_{s\in\left[t_{n-1},t_n\right]}\left|\frac{\partial^2\boldsymbol{y}}{\partial t^2}\left(x_i,s\right)\right| \le \boldsymbol{C}M^{-1}.$$

Further, we make use of (14)–(15) and the derivative bounds on the smooth component to bound the term $\mathcal{E}\left(\frac{\partial^2\boldsymbol{y}}{\partial x^2}-\delta_x^2\boldsymbol{y}\right)(x_i,t_n)$. We address the bound for $(x_i,t_n)\in G_1$; the corresponding bound for $(x_i,t_n)\in G_2$ can be proven in the same way. We consider the following three cases for G_1.

Case (i): Let $x_i\notin\left\{\sigma_{\varepsilon_s}^l, d-\sigma_{\varepsilon_s}^l\right\}$.

Using (15), we proceed as follows

$$\begin{aligned}\left|\varepsilon_m\left(\frac{\partial^2 y_m}{\partial x^2}-\delta_x^2 y_m\right)(x_i,t_n)\right| \quad &\le C\varepsilon_m(h_i+h_{i+1})^2\max_{s\in[x_{i-1},x_{i+1}]}\left|\frac{\partial^4 y_m}{\partial x^4}(s,t_n)\right|\\&\le C\varepsilon_m(h_i+h_{i+1})^2\max_{s\in[x_{i-1},x_{i+1}]}\left(1+\frac{B_{\varepsilon_m}^l(s)}{\varepsilon_m}\right).\end{aligned}$$

Note that $h_i+h_{i+1}\le CN^{-1}$, for all i. Therefore, we have

$$\left|\varepsilon_m\left(\frac{\partial^2 y_m}{\partial x^2}-\delta_x^2 y_m\right)(x_i,t_n)\right| \quad \le CN^{-2}.$$

Case (ii): Let $x_i\in\left\{\sigma_{\varepsilon_s}^l, d-\sigma_{\varepsilon_s}^l\right\}$, $m>s$. Here, the details for $x_i=\sigma_{\varepsilon_s}^l$ are provided; for $x_i=d-\sigma_{\varepsilon_s}^l$ the steps are analogous. Suppose h_{ε_s} and $h_{\varepsilon_{s+1}}$ are the mesh widths to the left and right of $\sigma_{\varepsilon_s}^l$, respectively.

Then, using (14) we proceed as follows

$$
\begin{aligned}
&\left|\varepsilon_m\left(\frac{\partial^2 y_m}{\partial x^2}-\delta_x^2 y_m\right)(x_i,t_n)\right| \quad \le C\varepsilon_m(h_i+h_{i+1})\max_{s\in[x_{i-1},x_{i+1}]}\left|\frac{\partial^3 y_m}{\partial x^3}(s,t_n)\right|\\
&\le C\varepsilon_m(h_{\varepsilon_s}+h_{\varepsilon_{s+1}})\max_{s\in[x_{i-1},x_{i+1}]}\left(1+\sum_{q=m}^{p}\frac{B^l_{\varepsilon_q}(s)}{\sqrt{\varepsilon_q}}\right)\\
&\le C\varepsilon_m(h_{\varepsilon_s}+h_{\varepsilon_{s+1}})\left(1+\sum_{q=m}^{p}\frac{B^l_{\varepsilon_q}(x_{i-1})}{\sqrt{\varepsilon_q}}\right)\\
&\le C\varepsilon_m(h_{\varepsilon_s}+h_{\varepsilon_{s+1}})\left(\sum_{q=m}^{p}\frac{1}{\sqrt{\varepsilon_q}}\right)\\
&\le C\varepsilon_m(h_{\varepsilon_s}+h_{\varepsilon_{s+1}})\frac{1}{\sqrt{\varepsilon_m}} \quad \left(\text{as } \frac{1}{\sqrt{\varepsilon_r}}<\frac{1}{\sqrt{\varepsilon_m}} \text{ for } \varepsilon_m<\varepsilon_r\right)\\
&\le C\sqrt{\varepsilon_m}(h_{\varepsilon_s}+h_{\varepsilon_{s+1}}).
\end{aligned}
$$

Case (iii): Let $x_i\in\left\{\sigma^l_{\varepsilon_s}, d-\sigma^l_{\varepsilon_s},\right\},\ m\le s.$

Using (14) and following the steps outlined in [8, Theorem 8.1], we obtain

$$
\left|\varepsilon_m\left(\frac{\partial^2 y_m}{\partial x^2}-\delta_x^2 y_m\right)(x_i,t_n)\right| \quad \le C\frac{\varepsilon_m}{\sqrt{\varepsilon_s}}(h_{\varepsilon_s}+h_{\varepsilon_{s+1}}).
$$

Thus, combining the above bounds, we have

$$
\begin{aligned}
&\left|\varepsilon_m\left(\frac{\partial^2 y_m}{\partial x^2}-\delta_x^2 y_m\right)(x_i,t_n)\right|\\
&\le\begin{cases}
CN^{-2} & \text{for } x_i\notin\left\{\sigma^l_{\varepsilon_s}, d-\sigma^l_{\varepsilon_s}, d+\sigma^r_{\varepsilon_s}, 1-\sigma^r_{\varepsilon_s}\right\},\\
C\left(\sqrt{\varepsilon_m}\left(h_{\varepsilon_s}+h_{\varepsilon_{s+1}}\right)\right) & \text{for } x_i\in\left\{\sigma^l_{\varepsilon_s}, d-\sigma^l_{\varepsilon_s}, d+\sigma^r_{\varepsilon_s}, 1-\sigma^r_{\varepsilon_s}\right\},\ m>s,\\
C\left(\frac{\varepsilon_m}{\sqrt{\varepsilon_s}}\left(h_{\varepsilon_s}+h_{\varepsilon_{s+1}}\right)\right) & \text{for } x_i\in\left\{\sigma^l_{\varepsilon_s}, d-\sigma^l_{\varepsilon_s}, d+\sigma^r_{\varepsilon_s}, 1-\sigma^r_{\varepsilon_s}\right\},\ m\le s.
\end{cases}
\end{aligned}
$$

Next, we proceed to estimate the truncation error for the singular component. We have

$$
\begin{aligned}
&\left(\boldsymbol{L}^{N,M}\boldsymbol{z}-\boldsymbol{L}\boldsymbol{z}\right)(x_i,t_n)\\
&=(D_t^- z-\frac{\partial z}{\partial t})(x_i,t_n)+\mathcal{E}\left(\frac{\partial^2 z}{\partial x^2}-\delta_x^2 z\right)(x_i,t_n)+\boldsymbol{\mathcal{N}}_i^n(z(x_i,t_n)-z(x_i,t_{n-1})).
\end{aligned}
$$

Using (12) and the bounds from Lemma 2 we get

$$
\left|(D_t^- z-\frac{\partial z}{\partial t})(x_i,t_n)+\boldsymbol{\mathcal{N}}_i^n(z(x_i,t_n)-z(x_i,t_{n-1}))\right|
$$

$$\leq C\tau \max_{s\in[t_{n-1},t_n]} \left| \frac{\partial^2 z}{\partial t^2}(x_i, s) \right| \leq \boldsymbol{C} M^{-1}.$$

The arguments for the term $\mathcal{E}\left(\frac{\partial^2 z}{\partial x^2} - \delta_x^2 z\right)(x_i, t_n)$ depend on the location of x_i. We bound this term in four cases as follows.

Case (i): Let $x_i \in \left[\sigma_{\varepsilon_p}^l, d - \sigma_{\varepsilon_p}^l\right] \cup \left[d + \sigma_{\varepsilon_p}^r, 1 - \sigma_{\varepsilon_p}^r\right]$. We consider the first half of the first interval, i.e., suppose $x_i \in \left[\sigma_{\varepsilon_p}^l, \frac{d}{2}\right]$. Then, from (13) and the derivative bounds on the layer components, we deduce that

$$\left| \varepsilon_m \left(\frac{\partial^2 z}{\partial x^2} - \delta_x^2 z \right)_m (x_i, t_n) \right| \leq C\varepsilon_m \sum_{q=m}^{p} \frac{B_{\varepsilon_q}^l(x)}{\varepsilon_q}$$
$$\leq C \left\| B_{\varepsilon_p}^l \right\|_{[x_{i-1}, x_{i+1}]} \leq CN^{-2}.$$

Similarly, we can prove the result for other half of the first interval, i.e., when $x_i \in [\frac{d}{2}, d - \sigma_{\varepsilon_p}^l]$. Further, similar arguments can be used to prove the result for $x_i \in [d + \sigma_{\varepsilon_p}^r, 1 - \sigma_{\varepsilon_p}^r]$. Thus, for $x_i \in [\sigma_{\varepsilon_p}^l, d - \sigma_{\varepsilon_p}^l] \cup [d + \sigma_{\varepsilon_p}^r, 1 - \sigma_{\varepsilon_p}^r]$, we have

$$\left| \varepsilon_m \left(\frac{\partial^2 z}{\partial x^2} - \delta_x^2 z \right)_m (x_i, t_n) \right| \leq CN^{-2}.$$

Case (ii): Next, suppose $x_i \in \left(0, \sigma_{\varepsilon_1}^l\right) \cup \left(d - \sigma_{\varepsilon_1}^l, d\right) \cup \left(d, d + \sigma_{\varepsilon_1}^r\right) \cup \left(1 - \sigma_{\varepsilon_1}^r, 1\right)$. Note that the mesh is equidistant in each interval. So, from (15), the mesh width and the derivative bounds on the layer component, we get

$$\left| \varepsilon_m \left(\frac{\partial^2 z}{\partial x^2} - \delta_x^2 z \right)_m (x_i, t_n) \right| \leq C \left(N^{-1} \ln N \right)^2.$$

Case (iii): Now, let $x_i \in (\sigma_{\varepsilon_s}^l, \sigma_{\varepsilon_{s+1}}^l) \cup (d - \sigma_{\varepsilon_{s+1}}^l, d - \sigma_{\varepsilon_s}^l) \cup (d + \sigma_{\varepsilon_s}^r, d + \sigma_{\varepsilon_{s+1}}^r) \cup (1 - \sigma_{\varepsilon_{s+1}}^r, 1 - \sigma_{\varepsilon_s}^r),\ 1 \leq s \leq p-1$. We use the singular components decomposition in Lemma 3 and derivative bounds to get

$$\left| \varepsilon_m \left(\frac{\partial^2 z}{\partial x^2} - \delta_x^2 z \right)_m (x_i, t_n) \right|$$
$$\leq \sum_{q=1}^{s} \varepsilon_m \left| \left(\frac{\partial^2}{\partial x^2} - \delta_x^2 \right) w_{m,\varepsilon_q}(x_i, t_n) \right| + \varepsilon_m \left| \left(\frac{\partial^2}{\partial x^2} - \delta_x^2 \right) w_{m,\varepsilon_{s+1}}(x_i, t_n) \right|. \tag{16}$$

Using the derivative bounds, the first term on the right-hand side of (16) yields

$$\sum_{q=1}^{s} \varepsilon_m \left| \left(\frac{\partial^2}{\partial x^2} - \delta_x^2 \right) w_{m,\varepsilon_q}(x_i, t_n) \right| \leq \sum_{q=1}^{s} \varepsilon_m \left\| \frac{\partial^2 w_{m,\varepsilon_q}}{\partial x^2}(., t_n) \right\|_{[x_{i-1}, x_{i+1}]}$$

$$\leq C B^l_{\varepsilon_s}(x_{i-1}) \leq C N^{-2}.$$

The second term is bounded using the derivative bounds and the mesh width definition as follows

$$\varepsilon_m \left| \left(\frac{\partial^2}{\partial x^2} - \delta_x^2 \right) w_{m,\varepsilon_{s+1}}(x_i, t_n) \right| \leq \frac{\varepsilon_m h_i^2}{12} \left\| \frac{\partial^4 w_{m,\varepsilon_{s+1}}}{\partial x^4} \right\| \leq C \left(N^{-1} \ln N \right)^2.$$

Thus, for $x_i \in (\sigma^l_{\varepsilon_s}, \sigma^l_{\varepsilon_{s+1}}) \cup (d - \sigma^l_{\varepsilon_{s+1}}, d - \sigma^l_{\varepsilon_s}) \cup (d + \sigma^r_{\varepsilon_s}, d + \sigma^r_{\varepsilon_{s+1}}) \cup (1 - \sigma^r_{\varepsilon_{s+1}}, 1 - \sigma^r_{\varepsilon_s})$, $1 \leq s \leq p-1$, we have

$$\left| \varepsilon_m \left(\frac{\partial^2 z}{\partial x^2} - \delta_x^2 z \right)_m (x_i, t_n) \right| \leq C \left(N^{-1} \ln N \right)^2.$$

Case (iv): Finally, suppose $x_i \in \left\{ \sigma^l_{\varepsilon_s}, d - \sigma^l_{\varepsilon_s}, d + \sigma^r_{\varepsilon_s}, 1 - \sigma^r_{\varepsilon_s} \right\}$, $1 \leq s \leq p-1$. We use the decomposition of z to get

$$\begin{aligned} &\left| \varepsilon_m \left(\frac{\partial^2 z}{\partial x^2} - \delta_x^2 z \right)_m (x_i, t_n) \right| \\ &\leq \sum_{q=1}^{s} \varepsilon_m \left| \left(\frac{\partial^2}{\partial x^2} - \delta_x^2 \right) z_{m,\varepsilon_q}(x_i, t_n) \right| + \varepsilon_m \left| \left(\frac{\partial^2}{\partial x^2} - \delta_x^2 \right) z_{m,\varepsilon_{s+1}}(x_i, t_n) \right|. \end{aligned} \tag{17}$$

Now, for $m \leq s$, using the definition of $x^{(m)}_{i,n}$ from Lemma 2.2 of [22] and previous arguments we get

$$\sum_{q=1}^{s} \varepsilon_m \left| \left(\frac{\partial^2}{\partial x^2} - \delta_x^2 \right) z_{m,\varepsilon_q}(x_i, t_n) \right| \leq \sum_{q=1}^{s} \varepsilon_m \left\| \frac{\partial^2 z_{m,\varepsilon_q}}{\partial x^2}(x_i, t_n) \right\|_{[x_{i-1}, x_{i+1}]} \leq C N^{-2}.$$

For $m > s$, using the derivative bounds and arguments as in the first case, we get

$$\sum_{q=1}^{s} \varepsilon_m \left| \left(\frac{\partial^2}{\partial x^2} - \delta_x^2 \right) z_{m,\varepsilon_q}(x_i, t_n) \right| \leq C N^{-2}.$$

The second term is bounded using the derivative bounds given in Lemma 3 as follows

$$\varepsilon_m \left| \left(\frac{\partial^2}{\partial x^2} - \delta_x^2 \right) z_{m,\varepsilon_{s+1}}(x_i) \right| \leq C \varepsilon_m \left(h_{\varepsilon_s} + h_{\varepsilon_{s+1}} \right) \left\| \frac{\partial^3 z_{m,\varepsilon_{s+1}}}{\partial x^3} \right\| \leq C \frac{\varepsilon_m}{\sqrt{\varepsilon_{s+1} \varepsilon_s}} N^{-1}.$$

Hence, for $x_i \in \left\{ \sigma^l_{\varepsilon_s}, d - \sigma^l_{\varepsilon_s}, d + \sigma^r_{\varepsilon_s}, 1 - \sigma^r_{\varepsilon_s} \right\}$, $1 \leq s \leq p-1$, we have

$$\varepsilon_m \left| \left(\frac{\partial^2 z}{\partial x^2} - \delta_x^2 z \right)_m (x_i, t_n) \right| \leq C \left(N^{-2} + \frac{\varepsilon_m}{\sqrt{\varepsilon_{s+1} \varepsilon_s}} N^{-1} \right).$$

At the point of discontinuity, $h_{\frac{N}{2}} = h_{\frac{N}{2}+1} = h$ and $\sigma^l_{\varepsilon_1} = \sigma^r_{\varepsilon_1} = 2\sqrt{\frac{\varepsilon_1}{\alpha}} \ln N$. Let the jump condition $-\varepsilon_m[\frac{\partial u_m}{\partial x}](d, t_n) = 0$ be approximated by the basic first order approximation, i.e., $-\varepsilon_m \left(D^+_x U_m - D^-_x U_m\right)(d, t_n) = 0$. In this case, the approximation error using Taylor expansions is given by

$$\begin{aligned}
e_m(d, t_n) &= -\varepsilon_m \left(D^+_x u_m - D^-_x u_m\right)(d, t_n) \\
&= -\varepsilon_m \Big(\Big(\frac{\partial u_m}{\partial x}(d+, t_n) + \frac{h}{2}\frac{\partial^2 u_m}{\partial x^2}(d+, t_n)\Big) - \Big(\frac{\partial u_m}{\partial x}(d+, t_n) \\
&\quad - \frac{h}{2}\frac{\partial^2 u_m}{\partial x^2}(d-, t_n)\Big)\Big) + O\left(h^2\right) \\
&= -\varepsilon_m \Big[\frac{\partial u_m}{\partial x}\Big](d, t_n) - \varepsilon_m \frac{h}{2}\frac{\partial^2 u_m}{\partial x^2}(d+, t_n) - \varepsilon_m \frac{h}{2}\frac{\partial^2 u_m}{\partial x^2}(d-, t_n) + O\left(h^2\right) \\
&= -\varepsilon_m \frac{h}{2}\frac{\partial^2 u_m}{\partial x^2}(d+, t_n) - \varepsilon_m \frac{h}{2}\frac{\partial^2 u_m}{\partial x^2}(d-, t_n) + O\left(h^2\right).
\end{aligned} \tag{18}$$

Using (1), we proceed considering two different cases as follows.
Case (i): When $\boldsymbol{\mathcal{M}}^n_i = diag(\boldsymbol{A}^n_i)$.
We get

$$\begin{aligned}
e_m(d, t_n) &= -\frac{h}{2}\frac{\partial u_m}{\partial t}(d, t_n) - \frac{h}{2}[a_{mm}u_m(d, t_n) + \sum_{r=1, r\neq m}^{p} a_{mr}u_r(d, t_{n-1})] \\
&\quad + \frac{h}{2}\bar{f}_m(d, t_n) + O\left(h^2\right) \\
&= -\frac{h}{2}D^-_t U_m(d, t_n) - \frac{h}{2}[a_{mm}u_m(d, t_n) + \sum_{r=1, r\neq m}^{p} a_{mr}u_r(d, t_{n-1})] \\
&\quad + \frac{h}{2}\bar{f}_m(d, t_n) + O\left(h^2 + \frac{h}{2}\tau\right).
\end{aligned}$$

Hence, in this case, the approximation of the jump condition $-\varepsilon_m[\frac{\partial u_m}{\partial x}](d, t_n) = 0$ is

$$\begin{aligned}
&\frac{h}{2}D^-_t U_m(x_i, t_n) - \frac{h}{2}\varepsilon_m \delta^2_x U_m(x_i, t_n) \\
&\qquad + \frac{h}{2}\left[a_{mm}u_m(d, t_n) + \sum_{r=1, r\neq m}^{p} a_{mr}u_r(d, t_{n-1})\right] \\
&\quad = \frac{h}{2}\bar{f}_m(x_i, t_n), \quad \text{for} \quad i = \frac{N}{2}, n > 0.
\end{aligned} \tag{19}$$

Case (ii): When $\boldsymbol{\mathcal{M}}^n_i = trial(\boldsymbol{A}^n_i)$.

We get

$$
\begin{aligned}
e_m(d,t_n) &= -\frac{h}{2}\frac{\partial u_m}{\partial t}(d,t_n) - \frac{h}{2}\left[\sum_{r=1}^{m} a_{mr}u_r(d,t_n) + \sum_{r=m+1}^{p} a_{mr}u_r(d,t_{n-1})\right] \\
&\quad + \frac{h}{2}\bar{f}_m(d,t_n) + O\left(h^2\right) \\
&= -\frac{h}{2}D_t^- U_m(d,t_n) - \frac{h}{2}\left[\sum_{r=1}^{m} a_{mr}u_r(d,t_n) + \sum_{r=m+1}^{p} a_{mr}u_r(d,t_{n-1})\right] \\
&\quad + \frac{h}{2}\bar{f}_m(d,t_n) + O\left(h^2 + \frac{h}{2}\tau\right).
\end{aligned}
$$

Hence, in this case, the approximation of the jump condition $-\varepsilon_m[\frac{\partial u_m}{\partial x}](d,t_n) = 0$ is

$$
\begin{aligned}
&\frac{h}{2}D_t^- U_m(x_i,t_n) - \frac{h}{2}\varepsilon_m\delta_x^2 U_m(x_i,t_n) \\
&\quad + \frac{h}{2}\left[\sum_{r=1}^{m} a_{mr}u_r(d,t_n) + \sum_{r=m+1}^{p} a_{mr}u_r(d,t_{n-1})\right] \\
&= \frac{h}{2}\bar{f}_m(x_i,t_n), \quad \text{for} \quad i = \frac{N}{2}, n > 0.
\end{aligned} \tag{20}
$$

Thus, the numerical error at this interface is $O\left(h^2 + \frac{h}{2}\tau\right)$. Dividing (19) and (20) by $\frac{h}{2}$ gives (8). Thus, at the interface $x = d$, for $1 \le m \le p$, we have

$$
\left|\left(\boldsymbol{L}^{N,M}(\boldsymbol{u} - \boldsymbol{U})\right)_m(d,t_n)\right| \le \left(M^{-1} + N^{-1}\ln N\right)C.
$$

We will now construct barrier functions for the truncation error. Start by defining $\phi_{1s}, \phi_{2s}, \phi_3, \phi_4$, $s = 1, 2, \ldots, p$, with

$$
\begin{aligned}
&\phi_{1s}(x_i) := \Pi_{k=1}^{i}\left(1 + \sqrt{\tfrac{\alpha}{2\varepsilon_s}}h_k\right), \quad \phi_{2s}(x_i) := \Pi_{k=1}^{i}\left(1 + \sqrt{\tfrac{\alpha}{2\varepsilon_s}}h_k\right)^{-1}, \\
&\phi_3(x_i) := \Pi_{k=1}^{i}\left(1 + \sqrt{\tfrac{\alpha}{2\varepsilon_1}}h_k\right), \quad \phi_4(x_i) := \Pi_{k=1}^{i}\left(1 + \sqrt{\tfrac{\alpha}{2\varepsilon_1}}h_k\right)^{-1}.
\end{aligned}
$$

Notice that,

$$D_x^- \phi_{1s}(x_i) = \frac{\sqrt{\alpha}}{\sqrt{2\varepsilon_s}\left(1+\sqrt{\alpha}h_i/\sqrt{2\varepsilon_s}\right)}\phi_{1s}(x_i), \qquad D_x^+ \phi_{1s}(x_i) = \frac{\sqrt{\alpha}}{\sqrt{2\varepsilon_s}}\phi_{1s}(x_i),$$
$$D_x^+ \phi_{2s}(x_i) = -\frac{\sqrt{\alpha}}{\sqrt{2\varepsilon_s}\left(1+\sqrt{\alpha}h_{i+1}/\sqrt{2\varepsilon_s}\right)}\phi_{2s}(x_i), \quad D_x^- \phi_{2s}(x_i) = -\frac{\sqrt{\alpha}}{\sqrt{2\varepsilon_s}}\phi_{2s}(x_i),$$
$$D_x^- \phi_3(x_i) = \frac{\sqrt{\alpha}}{\sqrt{2\varepsilon_1}\left(1+\sqrt{\alpha}h_i/\sqrt{2\varepsilon_1}\right)}\phi_3(x_i), \quad D_x^+ \phi_3(x_i) = \frac{\sqrt{\alpha}}{\sqrt{2\varepsilon_1}}\phi_3(x_i),$$
$$D_x^+ \phi_4(x_i) = -\frac{\sqrt{\alpha}}{\sqrt{2\varepsilon_1}\left(1+\sqrt{\alpha}h_{i+1}/\sqrt{2\varepsilon_1}\right)}\phi_4(x_i), \quad D_x^- \phi_4(x_i) = -\frac{\sqrt{\alpha}}{\sqrt{2\varepsilon_1}}\phi_4(x_i).$$

Further, we define $\eta_s, \eta_{sd}, \eta_d$, $s = 1, \ldots, p$ with

$$\eta_s(x_i) = \begin{cases} \frac{x_i}{\sigma^l_{\varepsilon_s}}, & 0 \le x_i \le \sigma^l_{\varepsilon_s}, \\ 1, & \sigma^l_{\varepsilon_s} \le x_i \le 1-\sigma^r_{\varepsilon_s}, \\ \frac{1-x_i}{\sigma^r_{\varepsilon_s}}, & 1-\sigma^r_{\varepsilon_s} \le x_i \le 1, \end{cases}$$
$$\eta_{sd}(x_i) = \begin{cases} \frac{\phi_{1s}(x_i)}{\phi_{1s}(d-\sigma^l_{\varepsilon_s})}, & 0 \le x_i \le d-\sigma^l_{\varepsilon_s}, \\ 1, & d-\sigma^l_{\varepsilon_s} \le x_i \le d+\sigma^r_{\varepsilon_s}, \\ \frac{\phi_{2s}(x_i)}{\phi_{2s}(d+\sigma^r_{\varepsilon_s})}, & d+\sigma^r_{\varepsilon_s} \le x_i \le 1, \end{cases}$$
$$\eta_d(x_i) = \begin{cases} \frac{\phi_3(x_i)}{\phi_3(d)}, & 0 \le x_i \le d, \\ \frac{\phi_4(x_i)}{\phi_4(d)}, & d \le x_i \le 1. \end{cases}$$

Now, for $i \ne \frac{N}{2}$, let

$$\Theta^{\pm}(x_i, t_n) = C\left(M^{-1} + \left(N^{-1}\ln N\right)^2\left(1+\sum_{s=1}^{p}\eta_s(x_i)+\eta_{sd}(x_i)\right)\right)(1,\ldots,1)^T \pm(\boldsymbol{U}-\boldsymbol{u})(x_i, t_n)$$

and, for $i = \frac{N}{2}$, let

$$\Theta^{\pm}(x_i, t_n) = C\left(M^{-1} + \left(N^{-1}\ln N\right)^2(1+\eta_d(x_i))\right)(1,\ldots,1)^T \pm(\boldsymbol{U}-\boldsymbol{u})(x_i, t_n).$$

Thus, the discrete maximum principle given in Lemma 4 with the barrier function $\Theta^{\pm}$ leads us to the following main theorem, proving the robust convergence of our proposed method.

Theorem 1 *Suppose $\boldsymbol{u}$ and $\boldsymbol{U}$ are the corresponding solution of the problem given by (1)–(2) and our proposed method described in the previous section respectively. Then*

$$\|\boldsymbol{u}-\boldsymbol{U}\|_{\overline{G}^{N,M}} \leq C\left(M^{-1}+\left(N^{-1}\ln N\right)^2\right).$$

5 Numerical experiments

Consider the following test examples with variable coefficients to illustrate the theoretical analysis in the preceding section and the efficacy of the proposed scheme. All the numerical results are recorded with MacBook Air Laptop with M1 Chip and 8GB RAM using MATLAB 2024a.

Example 1 Consider the problem

$$\begin{aligned}
&\frac{\partial u_1}{\partial t}-\varepsilon_1\frac{\partial^2 u_1}{\partial x^2}+4(1+xt)u_1-(2xt)u_2=f_1, \quad (x,t)\in G_1\cup G_2,\\
&\frac{\partial u_2}{\partial t}-\varepsilon_2\frac{\partial^2 u_2}{\partial x^2}-(2xt)u_1+4(1+x^2)u_2=f_2, \quad (x,t)\in G_1\cup G_2,\\
&\boldsymbol{u}(x,0)=(x(1-x),x(1-x^2))^T,\\
&\boldsymbol{u}(0,t)=(t^3,2t)^T \quad \text{and} \quad \boldsymbol{u}(1,t)=(1-\exp(-t),(1-\exp(-t))^2)^T,
\end{aligned}$$

where

$$f_1(x,t)=\begin{cases} t(1+2x), & 0\leq x\leq d,\\ -t, & d<x\leq 1\end{cases}$$

and

$$f_2(x,t)=\begin{cases} -t(3x+4), & 0\leq x\leq d,\\ 3t+2, & d<x\leq 1.\end{cases}$$

with $d=0.5$.

Example 2 Consider the problem

$$\begin{aligned}
&\frac{\partial u_1}{\partial t}-\varepsilon_1\frac{\partial^2 u_1}{\partial x^2}+5u_1-tu_2=f_1, \quad (x,t)\in G_1\cup G_2,\\
&\frac{\partial u_2}{\partial t}-\varepsilon_2\frac{\partial^2 u_2}{\partial x^2}-tu_1+5(1+xt)u_2-u_3=f_2, \quad (x,t)\in G_1\cup G_2,\\
&\frac{\partial u_3}{\partial t}-\varepsilon_3\frac{\partial^2 u_3}{\partial x^2}-2u_1-\left(1+x^2\right)u_2+(7+xt)u_3=f_3, \quad (x,t)\in G_1\cup G_2,\\
&\boldsymbol{u}(x,0)=\boldsymbol{0}, \quad \boldsymbol{u}(0,t)=\boldsymbol{0}, \quad \text{and} \quad \boldsymbol{u}(1,t)=\boldsymbol{0},
\end{aligned}$$

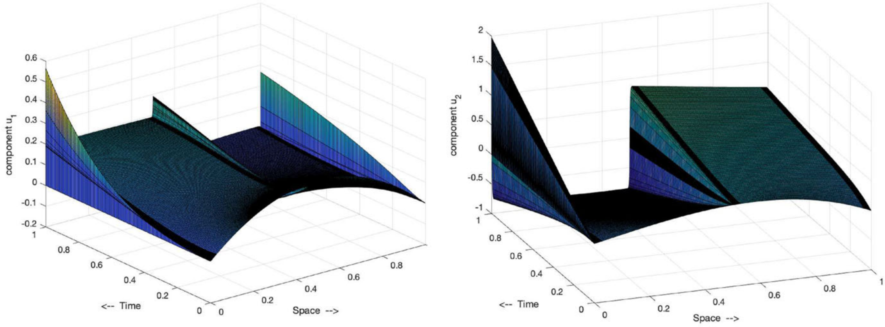

Fig. 1 Solution profile of u_1 and u_2 with $\boldsymbol{\mathcal{M}}_i^n = diag(\boldsymbol{A}_i^n)$ for Example 1 using the proposed additive scheme for $\varepsilon_1 = 10^{-9}$, and $\varepsilon_2 = 10^{-5}$ with $N = 512$, $M = 128$

where

$$f_1(x,t) = \begin{cases} 2 + x + t, & 0 \leq x \leq d, \\ 1, & d < x \leq 1, \end{cases}$$

$$f_2(x,t) = \begin{cases} 2, & 0 \leq x \leq d, \\ t, & d < x \leq 1 \end{cases}$$

and

$$f_3(x,t) = \begin{cases} (1+x), & 0 \leq x \leq d, \\ \left(x^2 + t\right), & d < x \leq 1. \end{cases}$$

with $d = 0.5$ or 0.2.

Taking $d = 0.5$, we analyze the surface plots of the solution. For both examples, the source function exhibits a jump discontinuity along the interface at $(\frac{1}{2}, t)$ for arbitrary t in the time domain. Figures 1 and 2 show the surface plots of each component of the solution of Examples 1 and 2 respectively, which clearly display boundary layers at both ends $x = 0, 1$ and interior layers near the discontinuity point $x = \frac{1}{2}$. We report the approximate solutions to these problems using the two proposed schemes and discuss the outcomes by comparing them with the standard method from [22].

As the analytical solutions for the given examples are unavailable, we estimate the errors by using a variant of the double mesh principle. So, we approximate the error $|\boldsymbol{S}^{i,n} - \boldsymbol{u}(x_i, t_n)|$, where $\boldsymbol{S}^{i,n}$ denotes the numerical solution calculated using the standard discretization on a piecewise uniform Shishkin mesh in space and uniform mesh in time, as

$$\boldsymbol{D}_{\boldsymbol{\varepsilon}}^{N,M} = \max_{0 \leq n \leq M} \max_{0 \leq i \leq N} |\boldsymbol{S}^{i,n} - \tilde{\boldsymbol{S}}^{2i,2n}|, \; \boldsymbol{D}^{N,M} = \max_{\boldsymbol{\varepsilon} \in R}(\boldsymbol{D}_{\boldsymbol{\varepsilon}}^{N,M}),$$

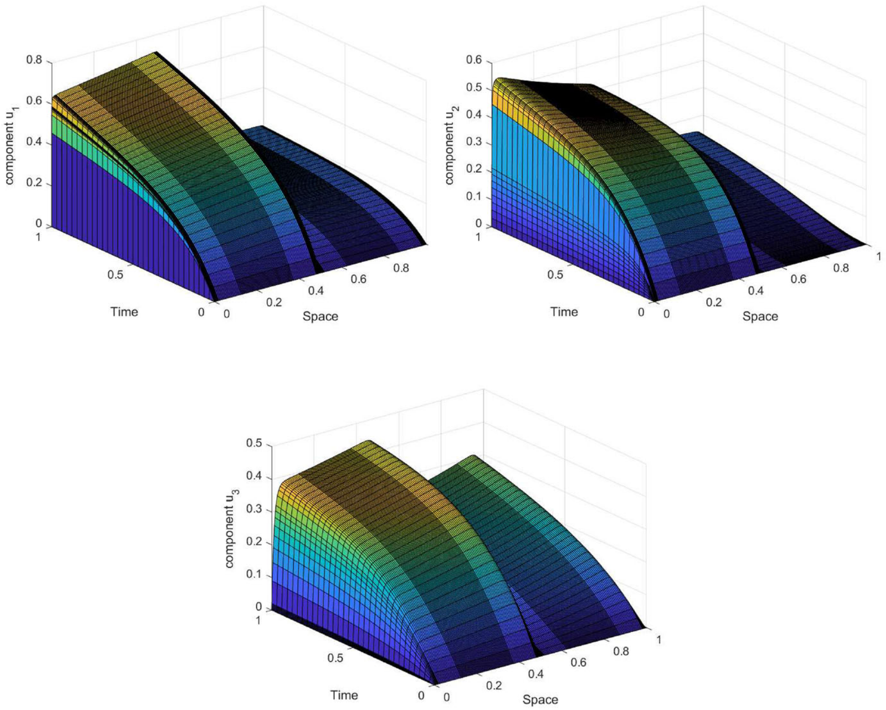

Fig. 2 Solution profile of u_1, u_2 and u_3 with $\boldsymbol{\mathcal{M}}_i^n = diag(\boldsymbol{A}_i^n)$ for Example 2 using the proposed additive scheme for $\varepsilon_1 = 10^{-8}$, $\varepsilon_2 = 10^{-5}$ and $\varepsilon_3 = 10^{-3}$ with $N = 256$, $M = 32$

where $\{\tilde{\boldsymbol{S}}^{i,n}\}$ denotes the solution on a fine mesh, i.e., on $\{(\tilde{x}_i, \tilde{t}_n)\}$ which is obtained by bisecting the original mesh, i.e.,

$$\begin{array}{llll} \widetilde{x}_{2i} = x_i, & i = 0, \ldots, N, & \widetilde{x}_{2i+1} = (x_i + x_{i+1})/2, & i = 0, \ldots, N-1, \\ \widetilde{t}_{2n} = t_n, & n = 0, \ldots, M, & \widetilde{t}_{2n+1} = (t_n + t_{n+1})/2, & n = 0, \ldots, M-1. \end{array} \tag{21}$$

For the numerical experiments, the following set of values were taken for Example 1

$$R = \{(\varepsilon_1, \varepsilon_2) : \varepsilon_1 = 10^{-m}, 1 \le m \le 10, \varepsilon_2 = 10^{-n}, 1 \le n \le m\}.$$

and for Example 2, values of the perturbation parameters were taken from the set

$$R' = \{(\varepsilon_1, \varepsilon_2, \varepsilon_3) : \varepsilon_1 = 10^{-m}, 1 \le m \le 10, \varepsilon_2 = 10^{-n}, 1 \le n \le m, \\ \varepsilon_3 = 10^{-o}, 1 \le o \le n\}.$$

We compute the order of convergence as

$$\boldsymbol{p} = \log_2\left(\boldsymbol{D}_{\boldsymbol{\varepsilon}}^{N,M}/\boldsymbol{D}_{\boldsymbol{\varepsilon}}^{2N,2M}\right), \ \boldsymbol{p}^{uni} = \log_2(\boldsymbol{D}^{N,M}/\boldsymbol{D}^{2N,2M}).$$

Table 1 Uniform error estimates $\widetilde{\boldsymbol{D}}^{N,M}$ and convergence rates $\widetilde{\boldsymbol{p}}^{uni}$ for Example 1 with $\alpha = 1.9$ and $d = 0.5$ using the scheme (6)–(9) with $\boldsymbol{\mathcal{M}}_i^n = diag(\boldsymbol{A}_i^n)$ as detailed out in (11)

	$N = 128$ $M = 2$	$N = 256$ $M = 8$	$N = 512$ $M = 32$	$N = 1024$ $M = 128$	$N = 2048$ $M = 512$
$\widetilde{D}_1^{N,M}$	4.6419e−02	1.9553e−02	6.4391e−03	2.0541e−03	6.1664e−04
$\widetilde{p}_1^{uni}$	1.247	1.602	1.648	1.736	
$\widetilde{D}_2^{N,M}$	5.6577e−02	1.9052e−02	5.3201e−03	1.3601e−03	3.5772e−04
$\widetilde{p}_2^{uni}$	1.570	1.840	1.968	1.927	

Table 2 Uniform error estimates $\widetilde{\boldsymbol{D}}^{N,M}$ and convergence rates $\widetilde{\boldsymbol{p}}^{uni}$ for Example 2 with $\alpha = 2.9$ and $d = 0.5$ using the scheme (6)–(9) with $\boldsymbol{\mathcal{M}}_i^n = diag(\boldsymbol{A}_i^n)$ as detailed out in (11)

	$N = 128$ $M = 2$	$N = 256$ $M = 8$	$N = 512$ $M = 32$	$N = 1024$ $M = 128$	$N = 2048$ $M = 512$
$\widetilde{D}_1^{N,M}$	5.4226e−02	2.3118e−02	8.9392e−03	2.8521e−03	8.4195e−04
$\widetilde{p}_1^{uni}$	1.230	1.371	1.648	1.760	
$\widetilde{D}_2^{N,M}$	6.5327e−02	2.6982e−02	8.4763e−03	2.2752e−03	5.8026e−04
$\widetilde{p}_2^{uni}$	1.276	1.671	1.897	1.971	
$\widetilde{D}_3^{N,M}$	9.6375e−02	3.7162e−02	1.1502e−02	3.0722e−03	7.8236e−04
$\widetilde{p}_3^{uni}$	1.375	1.692	1.905	1.973	

We find the approximate solution of the concerned test problems using our two proposed schemes and denote the discrete solution by $\boldsymbol{U}^{i,n}$. Using the double-mesh principle, the numerical errors are estimated as

$$\widetilde{\boldsymbol{D}}_{\boldsymbol{\varepsilon}}^{N,M} = \max_{0\leq n\leq M} \max_{0\leq i\leq N} |\boldsymbol{U}^{i,n} - \widetilde{\boldsymbol{U}}^{2i,2n}|,$$

where $\{\widetilde{\boldsymbol{U}}^{i,n}\}$ denotes the solution found using our proposed schemes on the fine mesh (21). The uniform error estimate is denoted by $\widetilde{\boldsymbol{D}}^{N,M}$ and the corresponding uniform convergence rates by $\widetilde{\boldsymbol{p}}^{uni}$. In Tables 1 and 2, we record the uniform error estimates and uniform convergence rates for each component of the numerical solution associated to the spatial discretization for $\boldsymbol{\mathcal{M}}_i^n = diag(\boldsymbol{A}_i^n)$ (diagonal part of matrix $\boldsymbol{A}_i^n$), when the discretization parameters N, M are multiplied by 2 and 4, for Examples 1 and 2 respectively.

Similarly, the numerical results are obtained correspondingly when $\boldsymbol{\mathcal{M}}_i^n = tril(\boldsymbol{A}_i^n)$ (lower triangular part of $\boldsymbol{A}_i^n$) in Tables 3 and 4 for Examples 1 and 2 respectively.

We also report the numerical results for the implicit Euler scheme in Tables 5 and 6 for Examples 1 and 2 respectively. From them, we infer that our proposed schemes and the standard discretization achieve almost the same order of convergence. Notice from Tables 1–6 that we get similar maximum errors using the classical scheme and

Table 3 Uniform error estimates $\widetilde{\boldsymbol{D}}^{N,M}$ and convergence rates $\widetilde{\boldsymbol{p}}^{uni}$ for Example 1 with $\alpha = 1.9$ and $d = 0.5$ using the scheme (6)–(9) with $\boldsymbol{\mathcal{M}}_i^n = trial(\boldsymbol{A}_i^n)$ as detailed out in (11)

	$N = 128$ $M = 2$	$N = 256$ $M = 8$	$N = 512$ $M = 32$	$N = 1024$ $M = 128$	$N = 2048$ $M = 512$
$\widetilde{D}_1^{N,M}$	4.6194e−02	1.9553e−02	6.4391e−03	2.0541e−03	6.1664e−04
$\widetilde{p}_1^{uni}$	1.240	1.602	1.648	1.736	
$\widetilde{D}_2^{N,M}$	5.6440e−02	1.9009e−02	5.3077e−03	1.3566e−03	3.5724e−04
$\widetilde{p}_2^{uni}$	1.570	1.841	1.968	1.925	

Table 4 Uniform error estimates $\widetilde{\boldsymbol{D}}^{N,M}$ and convergence rates $\widetilde{\boldsymbol{p}}^{uni}$ for Example 2 with $\alpha = 2.9$ and $d = 0.5$ using the scheme (6)–(9) with $\boldsymbol{\mathcal{M}}_i^n = trial(\boldsymbol{A}_i^n)$ as detailed out in (11)

	$N = 128$ $M = 2$	$N = 256$ $M = 8$	$N = 512$ $M = 32$	$N = 1024$ $M = 128$	$N = 2048$ $M = 512$
$\widetilde{D}_1^{N,M}$	5.4624e−02	2.3116e−02	8.9386e−03	2.8519e−03	8.4194e−04
$\widetilde{p}_1^{uni}$	1.241	1.371	1.648	1.760	
$\widetilde{D}_2^{N,M}$	5.5247e−02	2.3358e−02	7.3774e−03	1.9785e−03	5.1260e−04
$\widetilde{p}_2^{uni}$	1.242	1.663	1.899	1.949	
$\widetilde{D}_3^{N,M}$	3.9781e−02	1.6270e−02	5.0131e−03	1.3354e−03	3.4001e−04
$\widetilde{p}_3^{uni}$	1.289	1.698	1.908	1.974	

Table 5 Uniform error estimates $\boldsymbol{D}^{N,M}$ and convergence rates $\boldsymbol{p}^{uni}$ for Example 1 with $\alpha = 1.9$ and $d = 0.5$ using the implicit Euler scheme, according to (10)

	$N = 128$ $M = 2$	$N = 256$ $M = 8$	$N = 512$ $M = 32$	$N = 1024$ $M = 128$	$N = 2048$ $M = 512$
$D_1^{N,M}$	3.6433e−02	1.9575e−02	6.4407e−03	2.0548e−03	6.1676e−04
p_1^{uni}	0.896	1.604	1.648	1.736	
$D_2^{N,M}$	5.6441e−02	1.9010e−02	5.3079e−03	1.3567e−03	3.5722e−04
p_2^{uni}	1.570	1.841	1.968	1.925	

the proposed schemes, respectively, that is,

$$\max\left\{\widetilde{D}_1^{N,M}, \widetilde{D}_2^{N,M}, \widetilde{D}_3^{N,M}\right\} \approx \max\left\{D_1^{N,M}, D_2^{N,M}, D_3^{N,M}\right\}$$

for every column of the table in concern.

From a numerical perspective, an important question is the influence of the discontinuity point on the results. Tables 7 and 8 present the results obtained by taking $d = 0.2$ for Example 2 when $\boldsymbol{\mathcal{M}}_i^n = diag(A_i^n)$ and $\boldsymbol{\mathcal{M}}_i^n = trial(A_i^n)$. We observe that the location of the discontinuity point does not significantly affect numerical accuracy.

Table 6 Uniform error estimates $\boldsymbol{D}^{N,M}$ and convergence rates $\boldsymbol{p}^{uni}$ for Example 2 with $\alpha = 2.9$ and $d = 0.5$ using the implicit Euler scheme, according to (10)

	$N = 128$ $M = 2$	$N = 256$ $M = 8$	$N = 512$ $M = 32$	$N = 1024$ $M = 128$	$N = 2048$ $M = 512$
$D_1^{N,M}$	4.4182e−02	2.2445e−02	8.8982e−03	2.8455e−03	8.4132e−04
p_1^{uni}	0.977	1.335	1.645	1.758	
$D_2^{N,M}$	3.8889e−02	1.8318e−02	6.2085e−03	1.7774e−03	4.7585e−04
p_2^{uni}	1.086	1.561	1.805	1.901	
$D_3^{N,M}$	3.5490e−02	1.5033e−02	4.6798e−03	1.2491e−03	3.1823e−04
p_3^{uni}	1.239	1.683	1.906	1.973	

Table 7 Uniform error estimates $\widetilde{\boldsymbol{D}}^{N,M}$ and convergence rates $\widetilde{\boldsymbol{p}}^{uni}$ for Example 2 with $\alpha = 2.9$ and $d = 0.2$ using the scheme (6)–(9) with $\boldsymbol{\mathcal{M}}_i^n = diag(\boldsymbol{A}_i^n)$ as detailed out in (11)

	$N = 128$ $M = 2$	$N = 256$ $M = 8$	$N = 512$ $M = 32$	$N = 1024$ $M = 128$	$N = 2048$ $M = 512$
$\widetilde{D}_1^{N,M}$	5.6734e−02	2.3103e−02	8.9367e−03	2.8513e−03	8.6749e−04
$\widetilde{p}_1^{uni}$	1.296	1.370	1.648	1.717	
$\widetilde{D}_2^{N,M}$	6.5327e−02	2.5579e−02	7.9372e−03	2.1252e−03	5.4179e−04
$\widetilde{p}_2^{uni}$	1.353	1.688	1.901	1.972	
$\widetilde{D}_3^{N,M}$	8.4566e−02	3.2060e−02	9.7406e−03	2.5966e−03	6.6066e−04
$\widetilde{p}_3^{uni}$	1.399	1.719	1.907	1.975	

Table 8 Uniform error estimates $\widetilde{\boldsymbol{D}}^{N,M}$ and convergence rates $\widetilde{\boldsymbol{p}}^{uni}$ for Example 2 with $\alpha = 2.9$ and $d = 0.2$ using the scheme (6)–(9) with $\boldsymbol{\mathcal{M}}_i^n = trial(\boldsymbol{A}_i^n)$ as detailed out in (11)

	$N = 128$ $M = 2$	$N = 256$ $M = 8$	$N = 512$ $M = 32$	$N = 1024$ $M = 128$	$N = 2048$ $M = 512$
$\widetilde{D}_1^{N,M}$	5.6459e−02	2.3102e−02	8.9361e−03	2.8512e−03	8.5929e−04
$\widetilde{p}_1^{uni}$	1.289	1.370	1.648	1.730	
$\widetilde{D}_2^{N,M}$	5.3912e−02	2.2179e−02	6.9294e−03	1.9358e−03	5.1248e−04
$\widetilde{p}_2^{uni}$	1.281	1.678	1.840	1.917	
$\widetilde{D}_3^{N,M}$	3.3036e−02	1.3229e−02	4.0413e−03	1.0762e−03	2.7398e−04
$\widetilde{p}_3^{uni}$	1.320	1.711	1.909	1.974	

Further, Table 9 shows the computational time (in seconds) needed to compute the numerical error for Example 1 with different values of the perturbation parameters. We observe that the total computational cost is comparatively much lower for the proposed schemes than the classical approach, representing that our proposed schemes outdo the classical Euler approach.

Table 9 Computational Time (in seconds) needed to report the numerical error for Example 1 with different mesh parameters N, M for $\varepsilon_1 = 10^{-9}$ and $\varepsilon_2 = 10^{-5}$

Scheme	$N = 128$ $M = 2$	$N = 256$ $M = 8$	$N = 512$ $M = 32$	$N = 1024$ $M = 128$	$N = 2048$ $M = 512$
$\mathcal{M}_i^n = A_i^n$	0.273	0.965	12.440	320.261	9822.744
$\mathcal{M}_i^n = diag(A_i^n)$	0.087	0.362	1.108	14.919	190.921
$\mathcal{M}_i^n = trial(A_i^n)$	0.057	0.102	0.804	12.171	191.638

Table 10 Computational Time (in seconds) needed to report the numerical error for Example 2 with $d = 0.5$ and different parameters N, M for $\varepsilon_1 = 10^{-8}$, $\varepsilon_2 = 10^{-5}$ and $\varepsilon_3 = 10^{-3}$

Scheme	$N = 128$ $M = 2$	$N = 256$ $M = 8$	$N = 512$ $M = 32$	$N = 1024$ $M = 128$	$N = 2048$ $M = 512$
$\mathcal{M}_i^n = A_i^n$	0.349	2.139	40.082	1035.682	12622.140
$\mathcal{M}_i^n = diag(A_i^n)$	0.257	1.677	15.405	372.100	730.477
$\mathcal{M}_i^n = trial(A_i^n)$	0.273	1.582	15.084	369.228	728.498

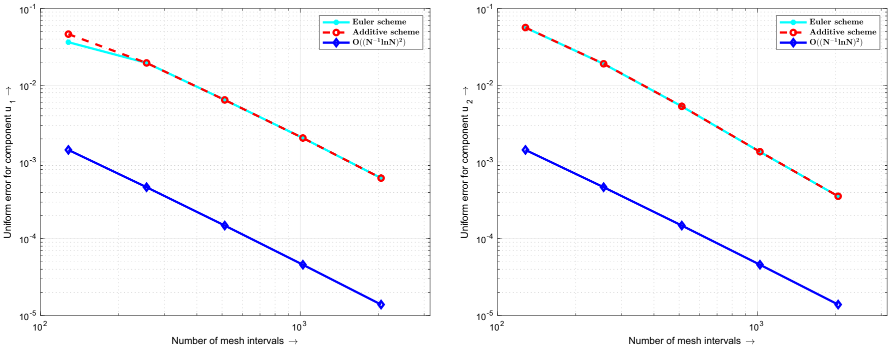

Fig. 3 Loglog plot of the uniform errors for each component of Example 1 for $\mathcal{M}_i^n = A_i^n$ (Euler) and $\mathcal{M}_i^n = diag(A_i^n)$ (Additive)

This decrease in the CPU time is more evident in Table 10, which we have recorded for the second Example consisting of more number of components. It clearly validates the efficiency of the proposed schemes in terms of computational cost reduction.

We have added the loglog plots of the uniform errors for each component of the numerical solution of Examples 1 and 2 in Figs. 3 and 4 respectively. From them, we notice that the slopes of these plots align with the theoretical order plots, supporting the robustness of our theoretical results. Moreover, we have added the error plots of the solution's components for both examples in Figs. 5 and 6, illustrating increased errors near the layer regions and decreased errors away from them. Also, the plot of the components of the numerical solution have also been provided in Fig. 7 by fixing time and varying perturbation parameters for Example 2 to observe the layer phenomena

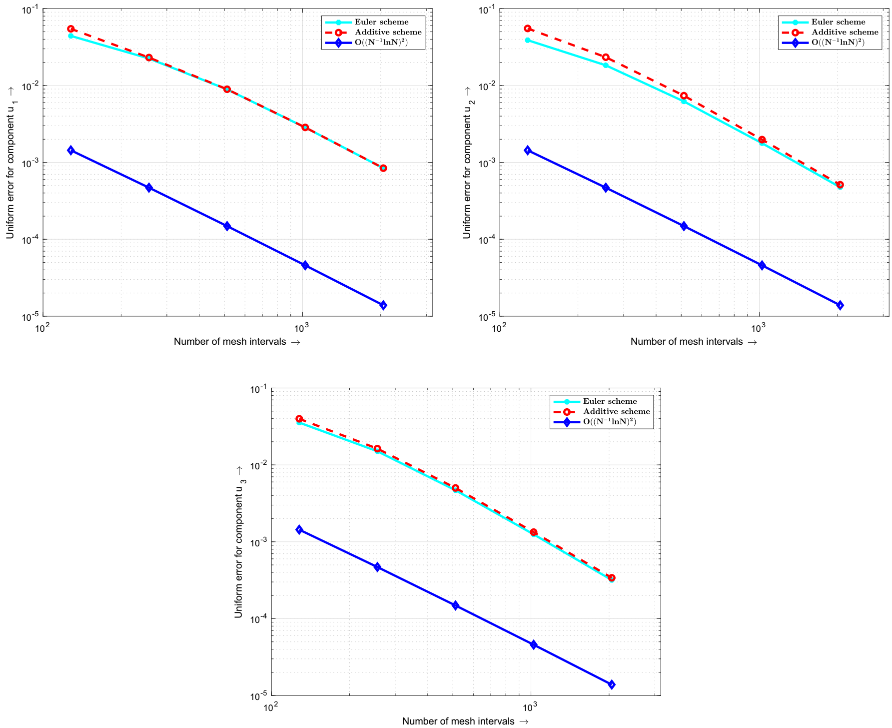

Fig. 4 Loglog plot of the uniform errors for each component of Example 2 with $d = 0.5$ for $\boldsymbol{\mathcal{M}}_i^n = \boldsymbol{A}_i^n$ (Euler) and $\boldsymbol{\mathcal{M}}_i^n = trial(\boldsymbol{A}_i^n)$ (Additive)

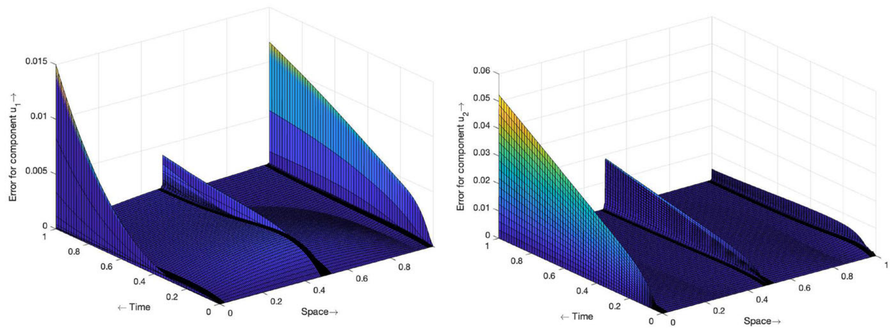

Fig. 5 Error plots for Example 1 when $\boldsymbol{\mathcal{M}}_i^n = diag(\boldsymbol{A}_i^n)$ with $N = 256$ and $M = 64$ for $\varepsilon_1 = 10^{-8}$ and $\varepsilon_2 = 10^{-5}$

in the solution. From this plot, we observe that as the magnitude of the perturbation parameters decreases the formation of the layer is noticeably sharper.

Next, if we consider the 1D system of equations corresponding to the standard discretization at the time level t_n for Example 2, then the ordering of the unknowns is

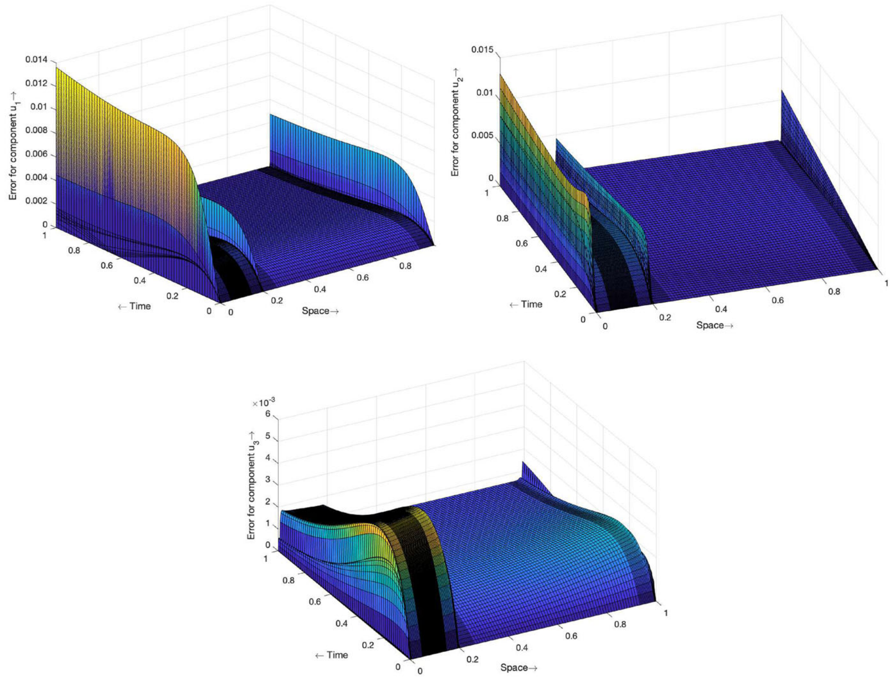

Fig. 6 Error plots for Example 2 when $\mathcal{M}_i^n = diag(\boldsymbol{A}_i^n)$ with $d = 0.2$, $N = 256$ and $M = 64$ for $\varepsilon_1 = 10^{-10}$, $\varepsilon_2 = 10^{-6}$ and $\varepsilon_3 = 10^{-4}$

as follows:

$$\boldsymbol{S}^n = \left(S_{1,1}^n, S_{1,2}^n, \dots, S_{1,N-1}^n, S_{2,1}^n, S_{2,2}^n, \dots, S_{2,N-1}^n, S_{3,1}^n, S_{3,2}^n, \dots, S_{3,N-1}^n\right)^T,$$

and the corresponding matrix of the system for the standard Euler scheme possesses the structure:

$$\begin{pmatrix} Q_1 & D_1 & R_1 \\ D_2 & Q_2 & P_1 \\ R_3 & P_2 & Q_3 \end{pmatrix},$$

where Q_s, with $s = 1, 2$ and 3 are tridiagonal matrices of order $N-1$, and D_s, R_s and P_s for $s = 1$, 2 and 3 represent diagonal matrices with the same order, with respective elements

$$(D_s)_{i,i} = a_{s(3-s)}(x_i, t_n), (Q_s)_{i,i} = \frac{2\varepsilon_s}{h_i h_{i+1}} + a_{ss}(x_i, t_n) + \frac{1}{\tau},$$
$$(R_s)_{i,i} = a_{s(4-s)}(x_i, t_n), (P_s)_{i,i} = a_{(s+1)(4-s)}(x_i, t_n),$$
$$(Q_s)_{i,i-1} = \frac{-\varepsilon_s}{h_i \bar{h}_i}, (Q_s)_{i,i+1} = \frac{-\varepsilon_s}{h_{i+1} \bar{h}_i}.$$

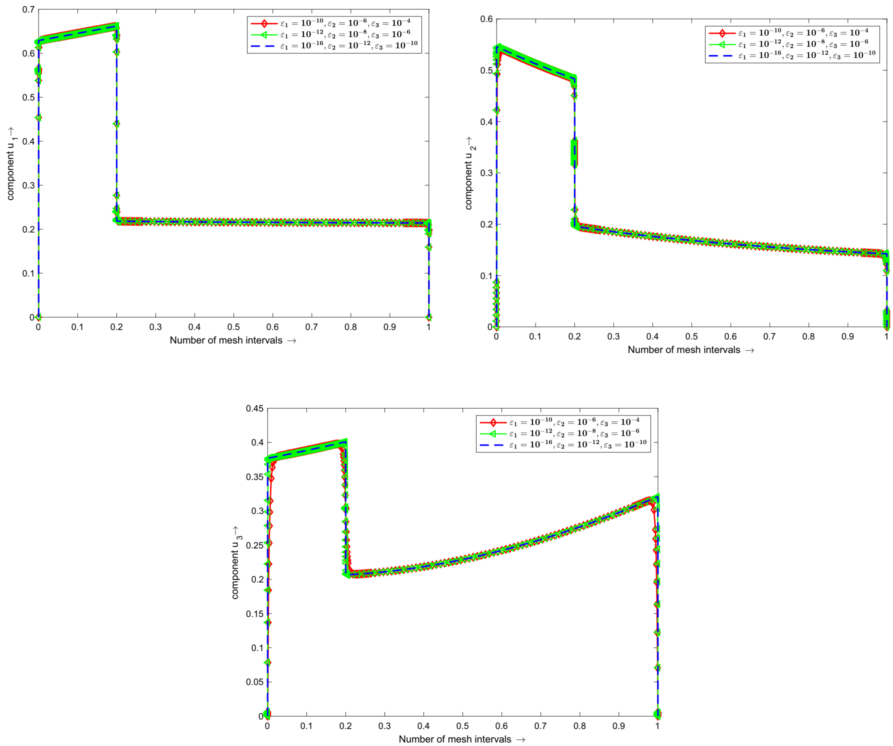

Fig. 7 Components the solution of Example 2 for $\boldsymbol{\mathcal{M}}_i^n = trial(\boldsymbol{A}_i^n)$ with $d = 0.2$, $N = 256$, $M = 8$ and $T = 1$

For the proposed schemes the coefficient matrices of the system possess the structure:

$$\begin{pmatrix} Q_1 & & \\ & Q_2 & \\ & & Q_3 \end{pmatrix}, \quad \begin{pmatrix} Q_1 & & \\ D_2 & Q_2 & \\ R_3 & P_2 & Q_3 \end{pmatrix},$$

when

$$\boldsymbol{\mathcal{M}}_i^n = \begin{pmatrix} a_{11}(x_i, t_n) & 0 & 0 \\ 0 & a_{22}(x_i, t_n) & 0 \\ 0 & 0 & a_{33}(x_i, t_n) \end{pmatrix},$$

or

$$\boldsymbol{\mathcal{M}}_i^n = \begin{pmatrix} a_{11}(x_i, t_n) & 0 & 0 \\ a_{21}(x_i, t_n) & a_{22}(x_i, t_n) & 0 \\ a_{31}(x_i, t_n) & a_{32}(x_i, t_n) & a_{33}(x_i, t_n) \end{pmatrix},$$

such that for $s = 1, 2$ and 3 the matrices Q_s, D_s, R_s and P_s are as stated above. For the proposed schemes, the matrices addressed in this paper are defined in a way that at each discrete time level, the discrete solution components are decoupled, and thus, only three triangular systems need to be solved for Example 2. Therefore, we reach the conclusion that as the number of equations in the system increases, the implicit Euler scheme takes more CPU time in comparison to the proposed additive schemes. Hence, the proposed schemes are more efficient as we observe a notable speedup in our algorithm when the number of components, p increases.

6 Conclusions

In this article, we have proposed robust numerical techniques for solving a system of parabolic one-dimensional singularly perturbed reaction–diffusion equations, under the assumption that the source function exhibits a discontinuity at an interior point within the spatial domain. We have considered that the diffusion parameters in each equation differ and may possess varying orders of magnitude, leading the exact solution to show multiscale phenomena i.e., we observe overlapping and interacting boundary layers at the ends of the spatial domain and interior layers at the point of discontinuity. To address these challenges, we developed efficient numerical schemes by applying a central difference scheme on a variant of Shishkin mesh for spatial discretization and special difference schemes for time discretization on a uniform mesh. The proposed schemes achieve first-order accuracy in time and nearly second-order accuracy in space. By decoupling the components of the numerical solution, the schemes deliver significant computational efficiency, achieving a remarkable reduction in computational cost compared to the standard discretization methods based on the implicit Euler technique. This efficiency becomes even more pronounced as the number of components in the system increases.

In future work, we aim to extend the methodology introduced here to address nonlinear singularly perturbed parabolic problems.

Acknowledgements The first author expresses gratitude to the Indian Institute of Technology (BHU) for the assistance provided during the work tenure. Sunil Kumar extends thanks to the Science and Engineering Research Board (SERB) for awarding the research support grant CRG/2023/003228 for this work.

Funding Open Access funding provided thanks to the CRUE-CSIC agreement with Springer Nature.

Data availability Data availability is not applicable for this paper.

Declarations

Conflict of interest The authors have no relevant financial or non-financial interests to disclose.

References

1. Aakansha, Kumar, S., Ramos, H.: A rapidly converging domain decomposition algorithm for a time delayed parabolic problem with mixed type boundary conditions exhibiting boundary layers. J. Appl. Math. Comput. **70**, 1043–1067 (2024)
2. Aakansha, Singh, J., Kumar, S.: Additive schemes based domain decomposition algorithm for solving singularly perturbed parabolic reaction–diffusion systems. Comput. Appl. Math. **40**, 1–15 (2021)
3. De Falco, C., O'Riordan, E.: Interior layers in a reaction–diffusion equation with a discontinuous diffusion coefficient. Int. J. Numer. Anal. Model. **7**(3), 444–461 (2010)
4. Derzie, E.B., Munyakazi, J.B., Gemechu, T.: A parameter-uniform numerical method for singularly perturbed burgers' equation. Comput. Appl. Math. **41**, 247 (2022)
5. Dunne, R.K., O'Riordan, E.: Interior layers arising in linear singularly perturbed differential equations with discontinuous coefficients. In: Proceedings of the Fourth International Conference on Finite Difference Methods: Theory and Applications, Lozenetz, Bulgaria, pp. 29–38 (2006)
6. Farrell, P., Hegarty, A., Miller, J.J.H., O'Riordan, E., Shishkin, G.I.: Robust Computational Techniques For Boundary Layers. CRC Press (2000)
7. Farrell, P.A., Hegarty, A.F., Miller, J.J.H., O'Riordan, E., Shishkin, G.I.: Singularly perturbed convection–diffusion problems with boundary and weak interior layers. J. Comput. Appl. Math. **166**(1), 133–151 (2004)
8. Franklin, V., Paramasivam, M., Miller, J.J.H., Valarmathi, S.: Second order parameter-uniform convergence for a finite difference method for a singularly perturbed linear parabolic system. Int. J. Numer. Anal. Model. **10**(1), 178–202 (2013)
9. Gracia, J.L., Clavero, C.: Uniformly convergent additive finite difference schemes for singularly perturbed parabolic reaction–diffusion systems. Comput. Math. Appl. **67**, 655–670 (2014)
10. Gupta, V., Sahoo, S.K., Dubey, R.K.: Robust higher order finite difference scheme for singularly perturbed turning point problem with two outflow boundary layers. Comput. Appl. Math. **40**, 179 (2021)
11. Kadalbajoo, M.K., Gupta, V.: A brief survey on numerical methods for solving singularly perturbed problems. Appl. Math. Comput. **217**(8), 3641–3716 (2010)
12. Kumar, D., Deswal, K., Singh, S.: Wavelet-based approximation with nonstandard finite difference scheme for singularly perturbed partial integrodifferential equations. Comput. Appl. Math. **41**, 341 (2022)
13. Kumar, S., Aakansha, Singh, J., Ramos, H.: Parameter-uniform convergence analysis of a domain decomposition method for singularly perturbed parabolic problems with robin boundary conditions. J. Appl. Math. Comput. **69**, 2239–2261 (2023)
14. Kumar, S., Kumar, M.: High order parameter-uniform discretization for singularly perturbed parabolic partial differential equations with time delay. Comput. Math. Appl. **68**(10), 1355–1367 (2014)
15. Kumar, S., Singh, J., Kumar, M.: A robust domain decomposition method for singularly perturbed parabolic reaction–diffusion systems. J. Math. Chem. **57**, 1557–1578 (2019)
16. Mbayi, C.K., Munyakazi, J.B., Patidar, K.C.: A fitted numerical method for interior-layer parabolic convection–diffusion problems. Int. J. Comput. Methods **19**(10), 2250028 (2022)
17. Miller, J.J.H., O'riordan, E., Shishkin, G.I.: Fitted Numerical Methods for Singular Perturbation Problems: Error Estimates in the Maximum Norm for Linear Problems in One and Two Dimensions. World Scientific (1996)
18. Munyakazi, J.B., Patidar, K.C., Sayi, M.T.: A robust fitted operator finite difference method for singularly perturbed problems whose solution has an interior layer. Math. Comput. Simul. **160**, 155–167 (2019)
19. Priyadarshana, S., Mohapatra, J., Pattanaik, S.: Parameter uniform optimal order numerical approximations for time-delayed parabolic convection diffusion problems involving two small parameters. Comput. Appl. Math. **41**, 233 (2022)
20. Rao, S.C.S., Chawla, S.: Interior layers in coupled system of two singularly perturbed reaction-diffusion equations with discontinuous source term. In: Numerical Analysis and Its Applications: 5th International Conference, NAA 2012, Lozenetz, Bulgaria, June 15–20, 2012, Revised Selected Papers 5, pp. 445–453. Springer (2013)
21. Rao, S.C.S., Chawla, S.: Second order uniformly convergent numerical method for a coupled system of singularly perturbed reaction-diffusion problems with discontinuous source term. In: Boundary and Interior Layers, Computational and Asymptotic Methods-BAIL 2014, pp. 233–244. Springer (2015)

22. Rao, S.C.S., Chawla, S.: Numerical solution of singularly perturbed linear parabolic system with discontinuous source term. Appl. Numer. Math. **127**, 249–265 (2018)
23. Rao, S.C.S., Chawla, S., Chaturvedi, A.K.: Numerical analysis for a class of coupled system of singularly perturbed time-dependent convection–diffusion equations with a discontinuous source term. Numer. Methods Partial Differ. Equ. **2022**(38), 1437–1467 (2021)
24. Roos, H.G., Stynes, M., Tobiska, L.: Robust numerical methods for singularly perturbed differential equations. In; Springer Series in Computational Mathematics, 2nd edn. Springer, Berlin (2008)
25. Sahoo, S.K., Gupta, V.: Higher order robust numerical computation for singularly perturbed problem involving discontinuous convective and source term. Math. Methods Appl. Sci. **45**(8), 4876–4898 (2022)
26. Sahoo, S.K., Gupta, V.: An almost second-order robust computational technique for singularly perturbed parabolic turning point problem with an interior layer. Math. Comput. Simul. **211**, 192–213 (2023)
27. Samarskii, A.A., Vabishchevich, P.N.: Computational Heat Transfer: The Finite Difference Methodology. Wiley (1995)
28. Singh, S., Choudhary, R., Kumar, D.: An efficient numerical technique for two-parameter singularly perturbed problems having discontinuity in convection coefficient and source term. Comput. Appl. Math. **42**, 62 (2023)
29. Vabishchevich, P.N.: Additive schemes for certain operator-differential equations. Comput. Math. Math. Phys. **50**, 2033–2043 (2010)